



Break-away of South China from Gondwana: Insights from the Silurian high-Nb basalts and associated magmatic rocks in the Diancangshan-Ailaoshan fold belt (SW China)



Huichuan Liu ^{a,b,*}, Xiaoping Xia ^c, Chun-Kit Lai ^{d,e}, Chengshi Gan ^f, Yongzhi Zhou ^f, Pengpeng Huangfu ^g

^a State Key Laboratory of Petroleum Resources and Prospecting, China University of Petroleum, Beijing 102249, China

^b College of Geosciences, China University of Petroleum, Beijing 102249, China

^c State Key Laboratory of Isotope Geochemistry, Guangzhou Institute of Geochemistry, Chinese Academy of Sciences, Guangzhou 510640, China

^d Faculty of Science, Universiti Brunei Darussalam, Gadong BE1410, Brunei Darussalam

^e Centre of Excellence in Ore Deposits (CODES), University of Tasmania, Hobart, Tasmania 7001, Australia

^f School of Earth Science and Engineering, Sun Yat-Sen University, Guangzhou 510275, China

^g Key Laboratory of Computational Geodynamics, College of Earth Sciences, University of Chinese Academy of Sciences, Beijing 100049, China

ARTICLE INFO

Article history:

Received 2 June 2018

Accepted 10 August 2018

Available online 13 August 2018

Keywords:

High-Nb basalt

Diancangshan-Ailaoshan (SW China)

Proto-Tethys

Back-arc rifting

Silurian

Gondwana

ABSTRACT

The Diancangshan-Ailaoshan fold belt (Yunnan, SW China) represents the remnants of the once vast Ailaoshan Ocean, a branch or back-arc basin of the Eastern Paleotethys. However, when and how this ocean/back-arc basin opened, and rifted South China away from Gondwana are still unresolved. In this study, Ordovician-Silurian high-Nb basalts (HNBs; 420 Ma), Mg-rich andesite (435 Ma), high-Mg basalt (446 Ma) and I-type granite (423 Ma) were newly identified in the Diancangshan-Ailaoshan fold belt. The HNBs are alkaline with high TiO₂ (1.8–1.9 wt%) and Nb (16.9–23.1 ppm) contents, high Nb/U (36.8–39.1) and (Nb/Th)_{PM} (1.17–1.21) ratios, positive Nb-Ta anomalies (primitive mantle-normalized) and positive ε_{Nd(t)} values (+3.2). The HNBs were likely derived from an OIB/arc-mixed mantle source in the garnet stability field. The Mg-rich andesites are medium-K calc-alkaline andesite with negative ε_{Nd(t)} values (−10.1) and negative Nb-Ta anomalies. The magma was likely derived from a mixture of depleted mantle peridotites and subducted sediments under low pressure and high H₂O conditions. The high-Mg basalts are high-K calc-alkaline and characterized by high MgO contents (9.3–9.4 wt%; Mg[#] = ~70), high Cr (369–379 ppm) and low Al₂O₃ (13.6–13.9 wt%) contents. They were likely derived from an enriched mantle source metasomatized by marine sediment-derived fluids. The I-type granites show medium SiO₂ content (63.6 wt%), low A/CNK ratio (0.9) and negative ε_{Nd(t)} value (−9.8), and may have formed by the partial melting of meta-basalts. These HNB, Mg-rich andesite, high-Mg basalt and I-type granite were likely formed in an intracontinental back-arc rift setting. Integrated with our published detrital zircon U–Pb age and Lu–Hf isotope evidence, we propose that South China may have commenced its break-up from Gondwana in response to the Late Ordovician–Silurian (446–420 Ma) Proto-Tethyan subduction, which opened a back-arc basin along the Ailaoshan fold belt.

© 2018 Elsevier B.V. All rights reserved.

1. Introduction

The mainland Southeast Asia is composed of three major Gondwana-derived tectonic blocks (Sibumasu, Simao-Indochina and South China). These tectonic blocks are widely accepted to have rifted from the northern Gondwana margin during the Paleozoic, drifted across the Paleotethys and accreted onto the southern Eurasian margin in the Mesozoic (Fig. 1; e.g., Burritt et al., 2014; Zaw et al., 2014). Existence of the Devonian-Carboniferous ophiolites along the Jinshajiang-

Ailaoshan-Song Ma fold belts demonstrates that an ocean/back-arc basin had separated the South China and Simao-Indochina blocks when the former broke-away from Gondwana (Halpin et al., 2016; Jian et al., 2009; Lai et al., 2014a, 2014b). However, due to the strong Triassic (Indosinian) and Cenozoic (Himalayan) thermotectonic overprinting, when and how the initial break-up occurred are still uncertain. Some workers argued that the break-up may have occurred by back-arc spreading related to the east-dipping subduction (in present-day orientation) of the main Paleotethyan Ocean beneath Simao-Indochina (Fan et al., 2010; Metcalfe, 2002, 2006, 2013; Wang et al., 2000), whereas some others considered that the break-up commenced as an Atlantic-type seafloor spreading (Jian et al., 2009; Lai et al., 2014a, 2014b; Zi et al., 2012). Different initial break-up times have been

* Corresponding author at: State Key Laboratory of Petroleum Resources and Prospecting, China University of Petroleum, Beijing 102249, China.

E-mail address: liuhuichuan1986@126.com (H. Liu).

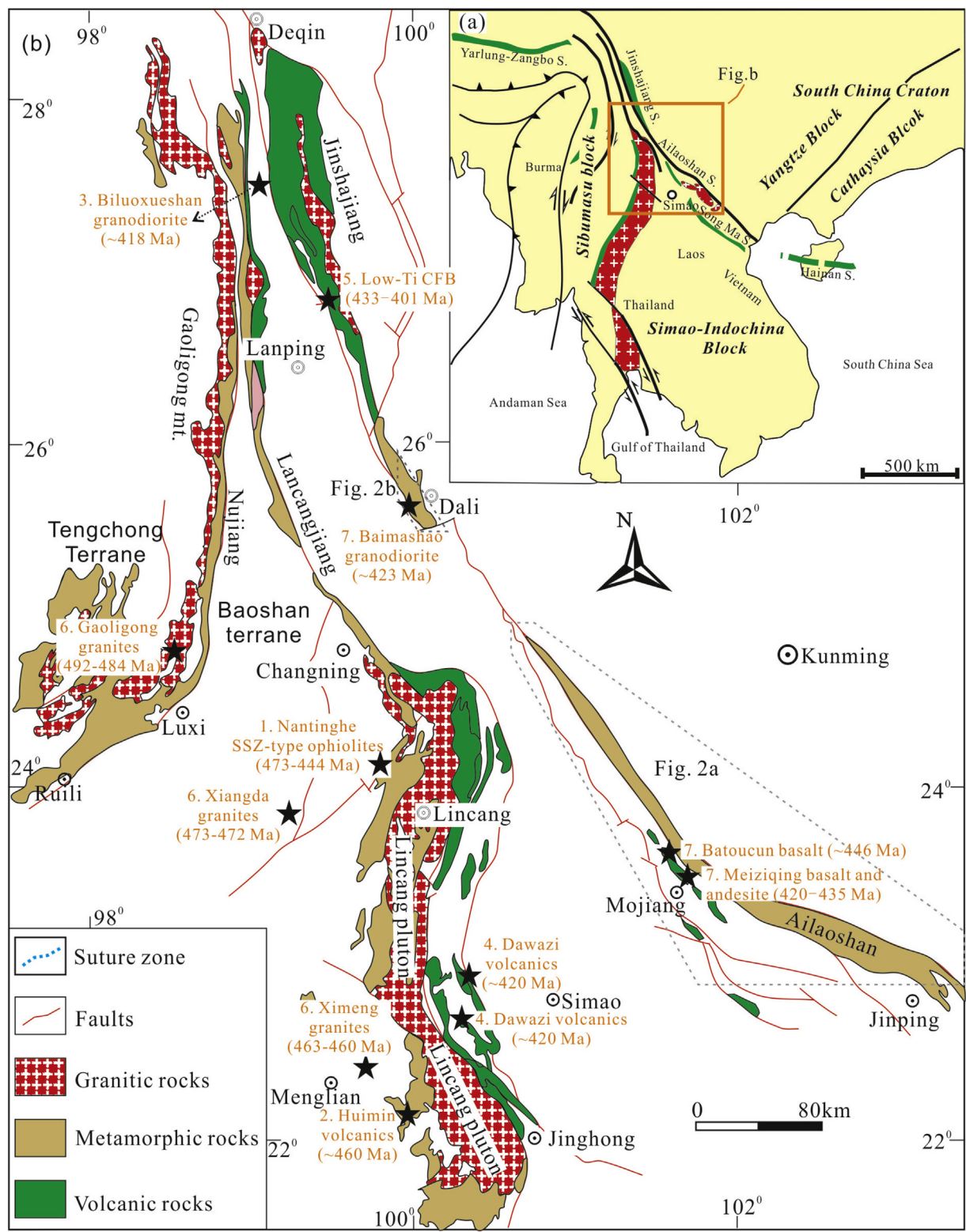


Fig. 1. (a) Tectonic outline of Southeast Asia (Wang et al., 2006), and (b) simplified geological map of the Yunnan province (China; Fan et al., 2010; Wang et al., 2006). Age data are from: 1- Wang et al. 2013a; 2- Xing et al. 2016 and Nie et al. 2015; 3- Mao et al. 2012; 4- Liu et al., in press b; 5- Jian et al. 2009; 6- Wang et al., 2013a; 7- This study.

proposed including Late Ordovician (Jian and Liu, 2002), Silurian (Jian et al., 2009; Xia et al., 2016), Early Carboniferous (Zi et al., 2012), and Middle Permian (Cheng and Shen, 1997; Fan et al., 2010).

Specific mafic rocks and rock associations are effective in tracing the nature of the mantle, geodynamic processes, and tectonic settings. High-Nb basalts (HNB) are uncommon mafic rocks characterized by

unusually high high-field strength elements (HFSE), particularly Nb (>18 ppm vs. ~4 ppm for typical arc basalts), and low LILE/HFSE and LREE/HREE ratios (Azizi et al., 2014; Castillo, 2008; Hastie et al., 2011; Macpherson et al., 2010; Mazhari, 2016). High-Nb basalts are commonly interpreted to be genetically linked to local or regional extension (Castillo, 2008; Macpherson et al., 2010). OIB (Ocean island basalt)-like

basalts have also been linked to localized and/or regional extension, e.g., mantle plumes or other types of upwelling asthenospheric mantle (Buiter and Torsvik, 2014; Niu et al., 2012; Zi et al., 2008). In this paper, we have newly identified coexisting HNBs and OIBs, and the associated Mg-rich andesite, high-Mg basalt and I-type granite in the Diancangshan-Ailaoshan fold belt (Fig. 1). Our new zircon U-Pb dating and geochemical analyses indicates that these specific mafic rocks were formed in the Late Ordovician to Silurian and have recorded the incipient rifting of South China from Simao-Indochina blocks.

2. Geological background and samples

In the Sanjiang (Chinese: three rivers, i.e., the Jinshajiang, Lancangjian and Nujiang rivers) region of SW Yunnan (Fig. 1b; YunnanBGMR 1990; Zhong 1998), the Lancangjiang fold belt is widely accepted to represent the main Proto-Tethys suture zone (between the Sibumasu and Simao-Indochina blocks), whilst the Jinshajiang-Ailaoshan fold belt (between the South China and Simao-Indochina blocks) is considered to represent a Paleo-Tethyan branch that was formed by back-arc spreading (Fan et al., 2010; Wang et al., in press; Fig. 1b). The western margin of the South China block consists of Archean to Paleoproterozoic crystalline basement and Neoproterozoic to lower Paleozoic and upper Paleozoic marine sedimentary assemblages (Wang et al., 2014, 2013a; Xia et al., 2016). Recently, middle Neoproterozoic volcanic arc rocks were also identified

in the Ailaoshan and Diancangshan complexes, probably representing a Neoproterozoic continental arc in the western margin of South China (Cai et al., 2015; Liu et al., 2014; Qi et al., 2012, 2014; Wang et al., 2016). The ~260 Ma Emeishan continental flood basalts, Triassic limestone and fine-grained clastic rocks, and Cretaceous terrestrial red beds overlie the lower Paleozoic sequences (Deng et al., 2014; Wang et al., 2007a).

The oldest rocks of the Indochina block are represented by the ca. 2.9 Ga (zircon U-Pb age) orthogenesis in northern Vietnam (Nam et al., 2003). Lower Paleozoic sequences of the Indochina block are similar to those of the South China block (Thanh et al., 1996), and are unconformably overlain by Middle Devonian basal conglomerates and shallow-marine sedimentary rocks, along with Carboniferous to Permian shallow-marine, paralic and continental successions (Metcalfe, 2006). These rocks are unconformably overlain by the Upper Triassic Gaoshanzhai and Waiguchun formations. Lower and Middle Triassic sequences are generally considered to be absent along the Jinshajiang-Ailaoshan-Song Ma fold belt (YunnanBGMR, 1990; Zhong, 1998).

In this study, two basalt (15YN-30C1 and 15YN-30C2) and one andesite samples (15YN-30B1) were collected from the Meiziqing area (Ailaoshan fold belt; Fig. 2b), and two basalt samples (15YN-35A and 15YN-35B) were collected from the Batoucun area (Ailaoshan fold belt; Fig. 2b). These basalts and andesites formed parts of the Ailaoshan ophiolites (Supplemental file 1). One granodiorite sample (15YN-65) was collected from the Baimashao area (Diancangshan fold belt; Fig.

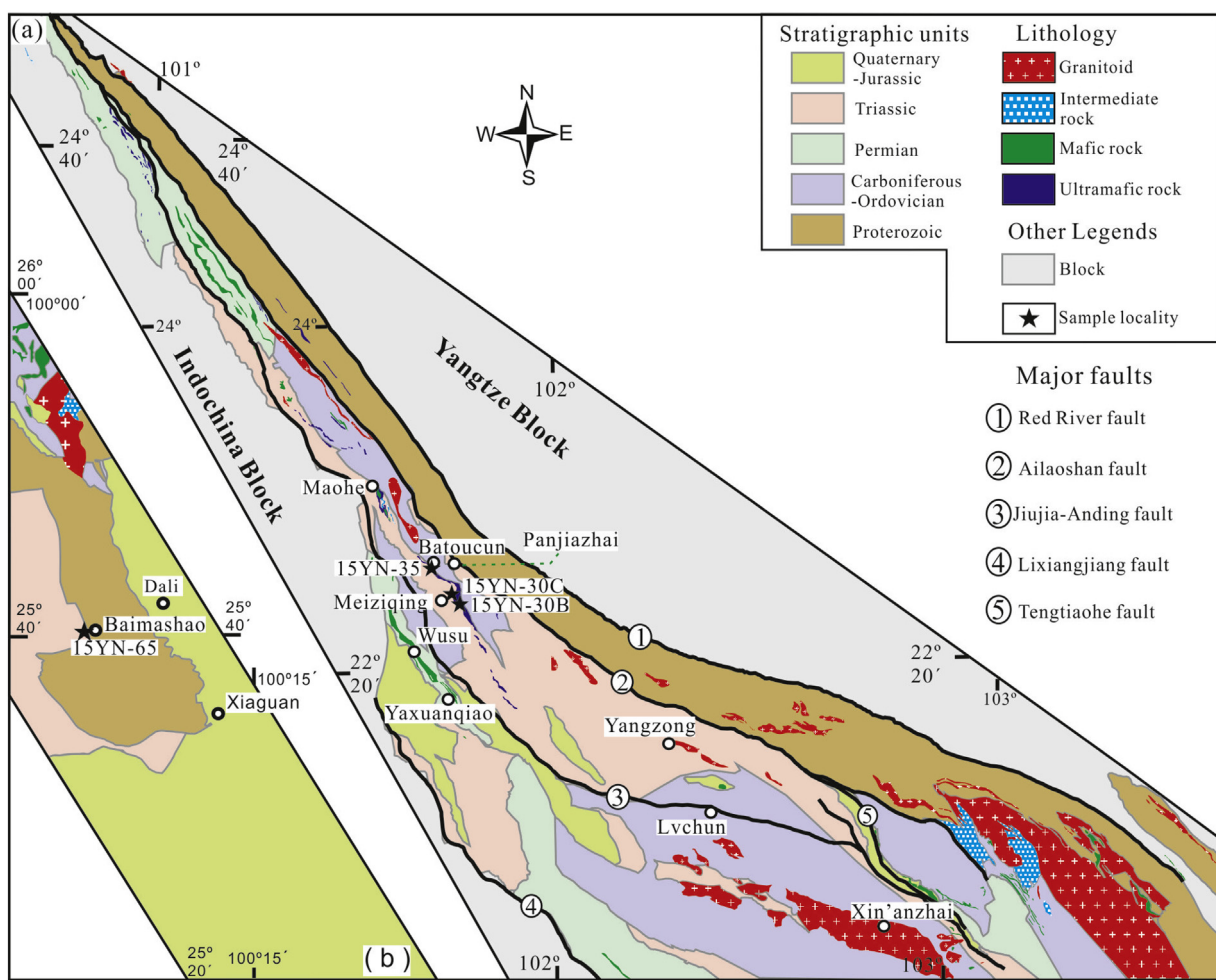


Fig. 2. (a) Tectonic outline of mainland Southeast Asia (Wang et al., 2006); (b) Simplified geological map of the Ailaoshan fold belt (YunnanBGMR, 1990); (c) Simplified geological map of the Diancangshan fold belt (YunnanBGMR, 1990).

Table 1

MC-ICP-MS zircon U–Pb dating results of the HNBs and associated magmatic rocks in the Diancangshan-Ailaoshan fold belt.

Spot	Th	U	Th/U	$^{207}\text{Pb}/^{235}\text{U}$	1sigma	$^{206}\text{Pb}/^{238}\text{U}$	1sigma	$^{207}\text{Pb}/^{235}\text{U}$	1sigma	$^{206}\text{Pb}/^{238}\text{U}$	1sigma
15YN-30B1-1	288	351	0.8	0.5381	0.0171	0.0696	0.0022	437	11	434	13
15YN-30B1-2	103	213	0.5	10.9674	0.3474	0.4685	0.0147	2520	30	2477	65
15YN-30B1-3	203	531	0.4	0.5306	0.0164	0.0700	0.0022	432	11	436	13
15YN-30B1-4	298	419	0.7	0.5330	0.0168	0.0695	0.0022	434	11	433	13
15YN-30B1-5	355	348	1.0	0.7373	0.0229	0.0907	0.0028	561	13	560	17
15YN-30B1-6	261	266	1.0	2.2069	0.0684	0.2025	0.0063	1183	22	1189	34
15YN-30B1-7	223	126	1.8	5.6883	0.1816	0.3352	0.0105	1930	28	1863	51
15YN-30B1-8	454	253	1.8	0.5329	0.0168	0.0698	0.0022	434	11	435	13
15YN-30B1-9	353	367	1.0	0.5677	0.0178	0.0692	0.0022	457	12	431	13
15YN-30B1-10	453	239	1.9	0.5660	0.0192	0.0706	0.0022	455	12	440	13
15YN-30B1-11	296	259	1.1	1.1992	0.0379	0.1312	0.0041	800	18	794	24
15YN-30B1-12	313	230	1.4	1.5414	0.0474	0.1576	0.0048	947	19	944	27
15YN-30B1-13	196	151	1.3	4.9187	0.1550	0.3227	0.0101	1805	27	1803	49
15YN-30B1-14	132	167	0.8	10.0688	0.3136	0.4473	0.0139	2441	29	2383	62
15YN-30B1-15	458	273	1.7	0.5278	0.0164	0.0696	0.0022	430	11	434	13
15YN-30B1-16	460	307	1.5	0.5794	0.0195	0.0707	0.0022	464	13	440	13
15YN-30B1-17	147	233	0.6	1.5992	0.0503	0.1597	0.0050	970	20	955	28
15YN-30B1-18	140	261	0.5	5.2803	0.1671	0.3359	0.0106	1866	27	1867	51
15YN-30B1-19	324	441	0.7	0.5292	0.0164	0.0696	0.0022	431	11	434	13
15YN-30B1-20	322	274	1.2	1.5848	0.0491	0.1562	0.0049	964	19	935	27
15YN-30C1-1	141	405	0.3	1.4686	0.0196	0.1527	0.0016	918	8	916	9
15YN-30C1-2	160	233	0.7	1.5111	0.0206	0.1540	0.0017	935	8	924	9
15YN-30C1-4	248	350	0.7	1.2842	0.0170	0.1345	0.0014	839	8	814	8
15YN-30C1-5	262	195	1.3	3.6091	0.0485	0.2666	0.0029	1552	11	1523	15
15YN-30C1-6	226	369	0.6	1.6209	0.0209	0.1666	0.0017	978	8	993	10
15YN-30C1-8	257	356	0.7	1.1134	0.0181	0.1249	0.0018	760	9	759	10
15YN-30C1-9	174	136	1.3	8.8760	0.1108	0.4018	0.0039	2325	11	2177	18
15YN-30C1-10	156	591	0.3	0.5160	0.0070	0.0670	0.0007	422	5	418	4
15YN-30C1-11	503	201	2.5	0.4975	0.0097	0.0676	0.0007	410	4	422	4
15YN-30C1-12	171	245	0.7	4.1152	0.0615	0.2910	0.0038	1657	12	1646	19
15YN-30C1-13	459	259	1.8	0.5237	0.0064	0.0678	0.0006	428	4	423	4
15YN-30C1-14	331	392	0.8	0.5114	0.0068	0.0670	0.0006	419	5	418	4
15YN-30C1-15	439	258	1.7	0.5099	0.0068	0.0667	0.0007	418	5	416	4
15YN-30C1-16	257	324	0.8	1.6897	0.0245	0.1663	0.0020	1005	9	992	11
15YN-30C1-17	351	180	2.0	1.0544	0.0140	0.1192	0.0013	731	7	726	7
15YN-30C1-18	379	304	1.2	0.5090	0.0086	0.0667	0.0010	418	6	416	6
15YN-30C1-19	313	431	0.7	0.5110	0.0074	0.0673	0.0006	419	5	420	4
15YN-30C1-20	419	270	1.6	0.5083	0.0072	0.0675	0.0008	417	5	421	5
15YN-35A-1	80	120	0.7	25.7132	1.3022	0.6096	0.0305	3336	50	3068	122
15YN-35A-2	104	428	0.2	2.5299	0.0842	0.2243	0.0072	1281	24	1305	38
15YN-35A-3	149	281	0.5	5.3476	0.1730	0.3423	0.0110	1876	28	1898	53
15YN-35A-4	463	237	2.0	0.5828	0.0201	0.0725	0.0025	466	13	451	15
15YN-35A-5	267	303	0.9	1.9087	0.0600	0.1823	0.0057	1084	21	1080	31
15YN-35A-6	210	195	1.1	4.9449	0.1555	0.3226	0.0101	1810	27	1802	49
15YN-35A-7	290	298	1.0	1.6149	0.0516	0.1616	0.0051	976	20	966	28
15YN-35A-8	332	127	2.6	0.5995	0.0255	0.0714	0.0023	477	12	445	13
15YN-35A-9	365	316	1.2	0.6052	0.0203	0.0735	0.0024	481	13	457	14
15YN-35A-10	507	212	2.4	0.5457	0.0170	0.0711	0.0022	442	11	443	13
15YN-35A-11	75	507	0.1	1.9532	0.0604	0.1910	0.0059	1100	21	1127	32
15YN-35A-12	437	318	1.4	0.5468	0.0176	0.0710	0.0023	443	12	442	14
15YN-35A-13	190	219	0.9	6.0993	0.2261	0.2945	0.0108	1990	32	1664	54
15YN-35A-14	361	373	1.0	0.5452	0.0174	0.0711	0.0022	442	11	443	13
15YN-35A-15	364	371	1.0	0.5472	0.0180	0.0711	0.0023	443	12	443	14
15YN-35A-16	134	186	0.7	10.6458	0.3299	0.4764	0.0147	2493	29	2511	64
15YN-35A-17	211	87	2.4	18.0743	0.6878	0.5187	0.0195	2994	37	2694	83
15YN-35A-18	480	195	2.5	0.5777	0.0201	0.0713	0.0022	463	13	444	13
15YN-35A-19	195	382	0.5	1.6350	0.0544	0.1654	0.0055	984	21	987	30
15YN-65-01	399	326	1.2	0.5227	0.0139	0.0682	0.0018	427	9	425	11
15YN-65-02	388	288	1.3	1.5482	0.0403	0.0927	0.0024	950	16	571	14
15YN-65-03	384	338	1.1	0.5125	0.0139	0.0669	0.0018	420	9	418	11
15YN-65-04	255	293	0.9	1.5378	0.0407	0.1563	0.0041	946	16	936	23
15YN-65-05	229	259	0.9	1.8874	0.0510	0.1850	0.0050	1077	18	1094	27
15YN-65-07	206	507	0.4	0.5182	0.0137	0.0680	0.0018	424	9	424	11
15YN-65-08	519	227	2.3	0.5187	0.0144	0.0675	0.0019	424	10	421	11
15YN-65-09	252	352	0.7	1.5792	0.0425	0.1578	0.0042	962	17	944	24
15YN-65-10	209	359	0.6	2.3491	0.0703	0.2253	0.0067	1227	21	1310	35
15YN-65-11	276	418	0.7	0.5217	0.0139	0.0678	0.0018	426	9	423	11
15YN-65-12	254	342	0.7	1.6426	0.0435	0.1577	0.0042	987	17	944	23
15YN-65-13	311	164	1.9	1.0238	0.0274	0.1169	0.0031	716	14	712	18
15YN-65-14	240	358	0.7	1.5329	0.0461	0.1561	0.0047	944	18	935	26
15YN-65-15	243	499	0.5	0.5363	0.0145	0.0683	0.0018	436	10	426	11
15YN-65-16	54	378	0.1	0.7134	0.0191	0.0883	0.0024	547	11	545	14

(continued on next page)

Table 1 (continued)

Spot	Th	U	Th/U	$^{207}\text{Pb}/^{235}\text{U}$	1sigma	$^{206}\text{Pb}/^{238}\text{U}$	1sigma	$^{207}\text{Pb}/^{235}\text{U}$	1sigma	$^{206}\text{Pb}/^{238}\text{U}$	1sigma
15YN-65-17	362	443	0.8	0.5214	0.0141	0.0676	0.0018	426	9	421	11
15YN-65-18	106	215	0.5	10.6506	0.2762	0.4692	0.0122	2493	24	2480	53
15YN-65-19	299	224	1.3	1.1492	0.0307	0.1265	0.0034	777	14	768	19
15YN-65-20	225	443	0.5	0.5201	0.0139	0.0678	0.0018	425	9	423	11

2c). The Meiziqing basalt is fine-grained with phenocrysts of plagioclase (5–10 vol%), clinopyroxene (10–15 vol%) and olivine (5–8 vol%). The groundmass consists of microcrystalline plagioclase (25–35 vol%), clinopyroxene (10–15 vol%), quartz (1–2 vol%), amphibole (1–5 vol%), biotite (1–5 vol%) and Fe-Ti oxides. The Meiziqing andesite is composed of plagioclase (~50 vol%), amphibole (~25 vol%), pyroxene (~20 vol%) and minor biotite (<5 vol%). The Batoucun basalt is mainly composed of ~30 vol% phenocrysts of clinopyroxene, plagioclase and orthopyroxene, and ~70 vol% groundmass of plagioclase, clinopyroxene, orthopyroxene, and amphibole. The Baimashao granodiorite contains ~30 vol% plagioclase, ~25 vol% quartz, ~15 vol% hornblende, ~15 vol% alkali feldspar, ~10 vol% biotite, and minor amount (<5 vol%) of magnetite, zircon and apatite. The sampling locations were shown in Fig. 2b and their field, hand specimen and petrographic thin section photos were shown in supplemental file 1.

3. Analytical methods

Zircons were extracted using conventional heavy liquid and magnetic separation techniques. They were then mounted in epoxy, polished and gold-coated for cathodoluminescence (CL) imaging at the Guangdong Key Laboratory of Mineral Resources and Geological Processes, Sun Yat-Sen University (Guangzhou, China).

Zircon U-Pb dating and trace element analyses were conducted using a Neptune plus multi-collector inductively coupled plasma mass spectrometer (LA-(MC)-ICP-MS) with RESolution M-50193 nm laser ablation system at the Guangzhou Institute of Geochemistry, Chinese Academy of Sciences (GIGCAS). The zircon standards 91500 and GJ were used to calibrate the U-Th-Pb ratios (Xia et al., 2013). The spot size for data collection was 30 μm . The errors for individual U-Pb analyses are presented with 1σ error and uncertainties in grouped ages are

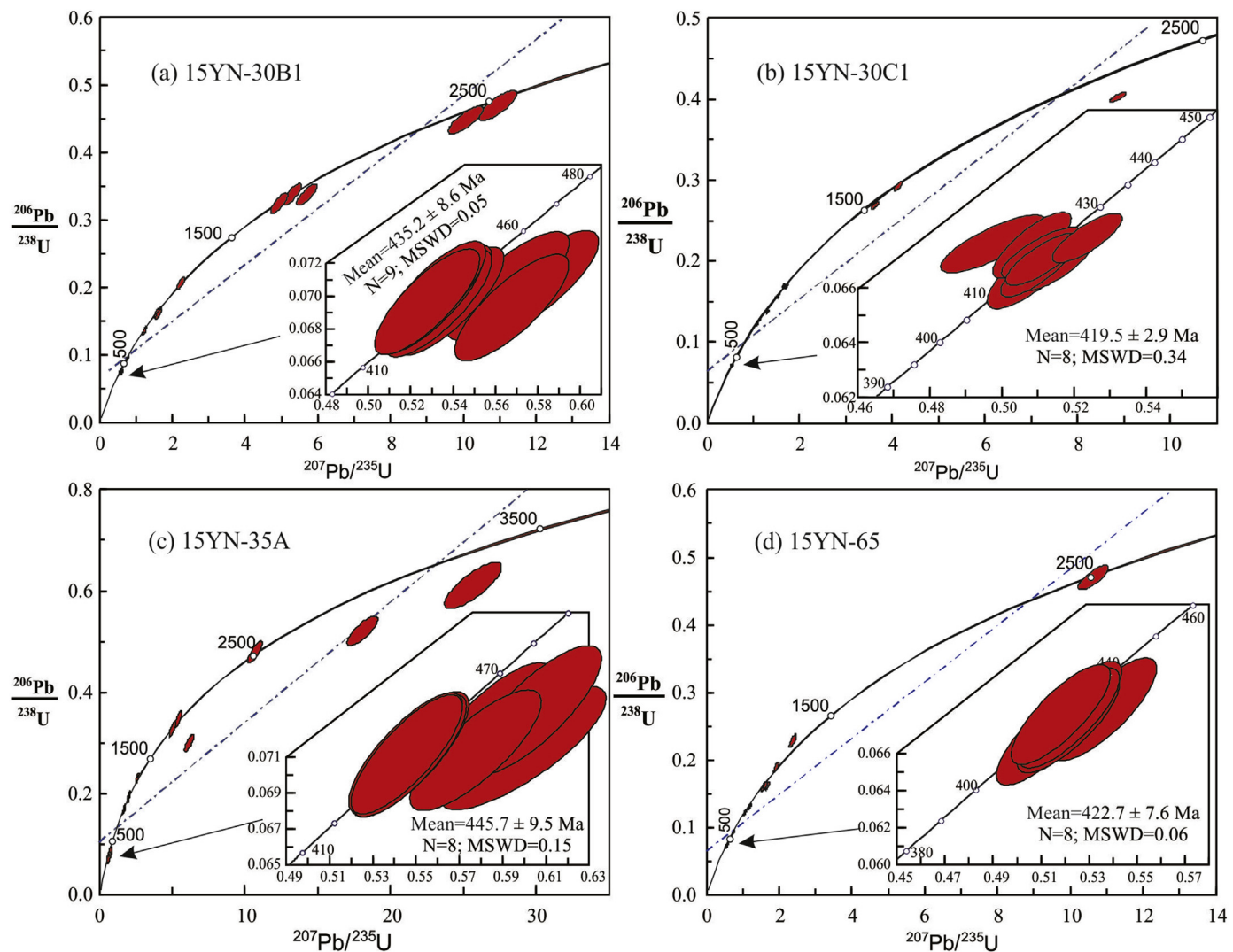


Fig. 3. LA-ICPMS zircon U-Pb concordia diagrams for the (a) Meiziqing andesite, (b) Meiziqing basalt, (c) Batoucun basalt and (d) Baimashao granodiorite.

quoted at 95% level (2σ). Off-line inspection and integration of background and analysis signals, and time-drift correction and quantitative calibration for trace element analyses and U-Pb dating were performed using ICPMSDataCal (Liu et al., 2008). Instrumentation and analytical procedure for the LA-ICP-MS zircon U-Pb dating and trace element analysis are similar to those described by Xia et al. (2013).

Samples for whole rock geochemistry and Sr-Nd isotopic analyses were crushed to 200-mesh using an agate mill. The major oxides were analyzed by a wavelength X-ray fluorescence spectrometer (XRF) at GIGCAS. Trace element analyses were performed at the GIGCAS using a Perkin-Elmer Sciex ELAN 6000 ICP-MS. Detailed sample preparation and analytical procedure followed those described in Li et al. (2012).

4. Results

4.1. Zircon U-Pb dating

Four samples (15YN-30B1, 15YN-30C1, 15YN-35A and 15YN-65) were collected for zircon U-Pb dating. The results are listed in Table 1 and the Concordia plots illustrated in Fig. 3. Cathodoluminescence (CL) images of the zircons are shown in Fig. 4.

4.1.1. Meiziqing andesite

Twenty zircon grains from sample 15YN-30B1 were dated. Eleven zircons yielded old $^{206}\text{Pb}/^{238}\text{U}$ apparent ages (560 to 2477 Ma) and are interpreted as inherited. The other nine zircons are euhedral, transparent to translucent, and prismatic/elongate in shape (100–200 μm long and 80–160 μm wide). Most of the zircons contain well-defined, broad oscillatory/sector zoning. The zoning pattern and the high Th/U ratios (0.4–1.9) suggest that these zircons are magmatic (Hanchar and Miller, 1993). These nine zircons yielded a weighted mean $^{206}\text{Pb}/^{238}\text{U}$ age of 435.2 ± 8.6 Ma [MSWD = 0.05, $n = 9$, Fig. 3a], representing the crystallization formation age of the andesite.

4.1.2. Meiziqing basalt

Twenty zircons were analyzed from sample 15YN-30C1. Twelve zircons yielded old $^{206}\text{Pb}/^{238}\text{U}$ apparent ages (726 to 2178 Ma), and are interpreted as inherited. The other eight zircons are subhedral (Figs. 4c). Most of the zircons contain distinct oscillatory/sector zoning. Some cores are dark under CL imaging, indicating high-U cores. The zoning pattern and high Th/U ratios (0.3–2.5) suggest that these zircons are magmatic (Hanchar and Miller, 1993). They yield $^{206}\text{Pb}/^{238}\text{U}$ ages of 416.0 to 422.9 Ma with a weighted mean age of 419.5 ± 2.9 Ma (MSWD = 0.34; Fig. 3b).

4.1.3. Batoucun basalt

Among the 19 zircons analyzed from sample 15YN-35A, 11 analyses yielded old $^{206}\text{Pb}/^{238}\text{U}$ apparent ages (966 to 3068 Ma) and are

interpreted as inherited zircons. The other eight zircons are euhedral, transparent to translucent, and elongate (80–120 μm long and 40–80 μm wide). The eight grains display well-developed oscillatory zoning and high Th/U ratios (1.0–2.6), typical of igneous zircon (Hanchar and Miller, 1993). They yielded a weighted mean $^{206}\text{Pb}/^{238}\text{U}$ age of 445.7 ± 9.5 Ma (MSWD = 0.15, $n = 8$, Fig. 3c), which is interpreted as the basalt formation age.

4.1.4. Baimashao granodiorite

Among the 20 magmatic zircons ($\text{Th}/\text{U} = 0.5$ –2.3) analyzed from sample 15YN-65, 12 zircons yielded much older $^{206}\text{Pb}/^{238}\text{U}$ apparent ages (545 to 2480 Ma), and are interpreted to be inherited. The other eight zircons yielded a weighted mean $^{206}\text{Pb}/^{238}\text{U}$ age of 422.7 ± 7.6 Ma (MSWD = 0.06; Fig. 3d), which is interpreted as the granodiorite emplacement age.

4.2. Whole-rock geochemistry

Whole-rock major oxides and trace element data for the studied samples are listed in Table 2. The two Meiziqing basalts display similar SiO_2 contents (45.6 and 46.1 wt%) and $\text{Mg}^{\#}$ ($100 \times [\text{atomic MgO}/(\text{MgO} + \text{FeO}_{\text{T}})]$) values (52.7). They contain high $\text{Na}_2\text{O} + \text{K}_2\text{O}$ (4.5 and 4.6 wt%) and TiO_2 (1.8 and 1.9 wt%), and are classified as alkali basalts (Fig. 5a). These basalts are also characterized by high Nb (16.9–23.1 ppm) contents and high Nb/U (36.8–39.1) and (Nb/Th)_{PM} (1.17–1.21) ratios (Fig. 5d). They have very uniform chondrite-normalized rare earth element (REE) patterns, no distinctive fractionation characteristics and negligible Eu anomalies ($\text{Eu}^* = 0.82$ –1.12; Fig. 6b). They show distinct chondrite-normalized LREE enrichments with unusually high $(\text{La/Yb})_{\text{N}}$ (6.1–8.4) and $(\text{La/Sm})_{\text{N}}$ (2.2–2.7) ratios. In the primitive mantle-normalized spider diagrams, the Meiziqing basalts show clear positive Nb and Ta anomalies (Fig. 6a). Such geochemical features resemble typical high-Nb basalts (HNBs; Azizi et al., 2014; Castillo, 2008; Hastie et al., 2011). The Meiziqing HNBs have $(^{87}\text{Sr}/^{86}\text{Sr})_{\text{i}}$ ratios of 0.71281 and positive $\epsilon_{\text{Nd}}(t)$ values of +3.2 (Fig. 7). By contrast, the Meiziqing andesite plots in the field of medium-K calc-alkaline series in Fig. 5b. The Meiziqing andesite shows low K_2O (1.1 wt%), but high MgO (4.2 wt%) and $\text{Mg}^{\#}$ (46), which is similar to the medium-K Mg-rich andesites in Yanhu area (southern Tibet; Fig. 5c; Li et al., 2018). The andesite sample has lower TiO_2 contents (0.92 wt%), negative Nb, Ta and Sr anomalies ($\text{Nb}^* = 0.14$; $\text{Sr}^* = 0.02$), and negative $\epsilon_{\text{Nd}}(t)$ values of −10.1 (Tables 2 and 3).

The Batoucun basalts were classified as high-K calc-alkaline basalt (Figs. 5a–b) and have low SiO_2 (49.3 and 50.8 wt%), high MgO (9.3 and 9.4 wt%), high $\text{Mg}^{\#}$ values (~70), low Al_2O_3 (13.6 and 13.9 wt%), high K_2O (1.6 and 1.7 wt%) and low TiO_2 (~0.9 wt%) (Table 2). They also show high Cr contents (379 and 369 ppm). These features are akin to the high-Mg basalt (Fig. 5d; e.g., Cervantes and Wallace, 2003;

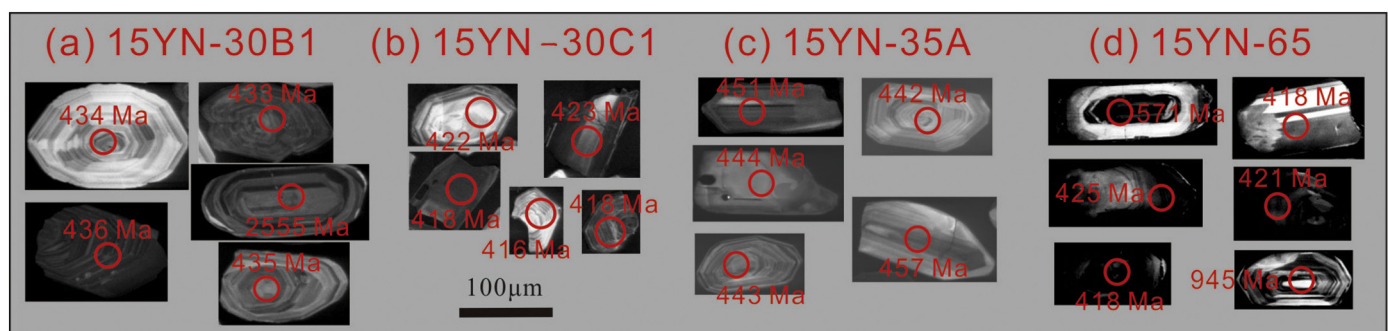


Fig. 4. Cathodoluminescence (CL) images of representative zircons. Red circles denote the laser spots.

Table 2

Major (wt%) and trace elemental (ppm) data of the HNBs and associated magmatic rocks in the Diancangshan-Ailaoshan fold belt.

Sample	15YN-30B1	15YN-30C1	15YN-30C2	15YN-35A	15YN-35B	15YN-65A	PJAB-1	PJAB-3	PJAB-4
SiO ₂	58.11	45.64	46.11	49.33	50.84	63.59	49.20	46.60	45.04
TiO ₂	0.92	1.81	1.92	0.90	0.93	0.59	2.72	2.73	2.33
Al ₂ O ₃	15.72	15.71	14.47	13.57	13.86	12.67	18.08	17.36	16.31
Fe ₂ O ₃ t	11.67	13.16	11.87	9.48	9.43	4.97	15.07	15.35	12.72
MnO	0.09	0.25	0.17	0.16	0.15	0.07	0.24	0.24	0.20
MgO	4.18	6.30	5.67	9.36	9.25	2.82	7.85	5.82	7.81
CaO	2.91	4.53	7.30	5.41	4.94	4.83	1.68	0.30	2.95
Na ₂ O	3.34	4.50	4.40	<0.1	0.17	0.96	1.40	0.59	2.02
K ₂ O	1.11	0.13	0.17	1.67	1.60	3.37	4.13	4.23	3.45
P ₂ O ₅	0.23	0.19	0.23	0.12	0.13	0.13	0.43	0.45	0.57
LOI	1.36	7.37	7.25	9.51	8.65	5.50			
Total	99.64	99.58	99.55	99.59	99.93	99.50			
V	53.3	329	277	220	229	113	428	507	349
Cr	51.3	429	248	379	369	78.5	201	268	133
Ga	6.36	20.5	19.8	17.5	17.8	15.5		26.3	18.3
Rb	46.3	3.39	5.84	96.7	93.7	180.5	89.2	92.5	85.9
Sr	7.00	181	286	83.0	81.0	111	87.4	181	151
Y	24.6	22.4	21.7	14.7	16.0	24.3	23.7	22.1	25.2
Zr	187	103	122	99.0	100	171	267	270	264
Nb	6.05	16.9	23.1	10.1	10.3	11.9	51.6	52.6	50.5
Cs	1.96	1.09	2.47	10.9	9.76	5.89			
Ba	235	165	254	205	199	440	798	638	957
La	21.8	13.8	18.4	17.5	16.6	35.6	52.6	52.7	52.6
Ce	40.4	28.8	35.8	35.7	34.2	72.2	112	111	114
Pr	4.66	3.60	4.30	3.78	3.63	7.46	13.0	13.2	12.8
Nd	18.6	15.9	17.9	14.9	14.9	28.6	48.4	50.7	46.0
Sm	3.95	3.97	4.39	3.01	3.21	5.49	8.04	8.09	7.99
Eu	0.840	1.14	1.67	0.780	0.850	1.18	2.46	2.53	2.38
Gd	4.03	4.50	4.71	2.88	3.13	4.57	6.54	6.70	6.38
Tb	0.540	0.660	0.660	0.450	0.480	0.650	0.970	1.00	0.939
Dy	3.59	4.14	4.27	2.66	2.83	4.01	5.30	5.21	5.39
Ho	0.780	0.820	0.810	0.570	0.600	0.830	0.996	1.00	0.991
Er	2.08	2.01	2.11	1.63	1.76	2.44	2.67	2.67	2.66
Tm	0.290	0.270	0.270	0.260	0.280	0.370	0.400	0.410	0.389
Yb	1.73	1.61	1.58	1.72	1.84	2.32	2.35	2.40	2.29
Lu	0.260	0.240	0.230	0.290	0.300	0.360	0.355	0.380	0.329
Hf	4.82	2.79	3.07	2.59	2.77	4.61	6.79	6.98	6.60
Ta	0.410	1.00	1.39	0.700	0.720	0.880	3.71	3.63	3.78
Th	7.71	1.67	2.36	5.76	5.80	13.5	10.7	11.2	10.1
U	1.50	0.460	0.590	1.45	1.44	2.65	1.70	1.84	1.55

Samples PJAB-1, PJAB-3 and PJAB-4 are from reference [Cheng and Shen \(1997\)](#).

[Mattioli et al., 2000](#); [Melluso et al., 2006](#); [Peng et al., 2013](#)). Compared to the Meiziqing HNBs, the Batoucun basalts contain lower TiO₂ (0.90–0.93) and Na₂O + K₂O contents, and with negative Nb, Ta and Sr anomalies (Nb* = 0.30; Sr* = 0.25; primitive mantle-normalized; [Tables 2](#) and [Fig. 6](#)). They have (⁸⁷Sr/⁸⁶Sr)i ratios of 0.71224 and negative ε_{ND}(t) values of −4.8 ([Fig. 7](#)).

The Baimashao granodiorite (sample 15YN-65) contain medium SiO₂ (63.6 wt%) and Al₂O₃ (12.7 wt%), and high K₂O contents (3.4 wt%, [Fig. 5b](#)). The samples are metaluminous (A/CNK (Al₂O₃/(CaO + Na₂O + K₂O)) value = 0.9), and contain no muscovite, cordierite or garnet. The samples have low FeO_T/MgO (1.6) and AI (molar (Na₂O + K₂O)/Al₂O₃) values (0.43) which are different from the A-type granites. These geochemical features are different from A-type but similar to I-type ([Chappell and White, 1992](#); [Kemp et al., 2005](#)). In the primitive mantle-normalized multi-element spidergram ([Fig. 6](#)), the Baimashao granodiorite exhibits strongly negative Nb, Ta, Ti and Sr anomalies. They show chondrite-normalized LREE-enrichments with moderate negative Eu anomalies (Eu* = 0.72; [Fig. 6d](#)). As shown in [Fig. 7](#), the Baimashao granodiorite is characterized by negative ε_{ND}(t) value of −9.8.

5. Discussion

5.1. Formation of the Meiziqing HNBs

Although the presence of inherited zircons in the Meiziqing HNBs indicates crustal contamination, such contamination was unlikely to be petrogenetically significant, because: (1) Crustal materials are marked

by extreme HFSE (incl. Nb and Ta) depletions, yet positive Nb-Ta anomalies are present in the Meiziqing HNBs ([Fig. 6a](#)); (2) The highly positive zircon ε_{ND}(t) values (+3.5) are inconsistent with crustal contamination ([Fig. 7](#)). The inherited zircons in the Meiziqing HNBs may have been from minor assimilation of sedimentary rocks which could contribute a disproportionately large number of zircons, but with negligible effect on the whole-rock element and isotope compositions ([Wang et al., 2008](#)).

Two petrogenetic models for HNBs have been proposed: (I) partial melting of mantle wedge metasomatized by adakitic melts (e.g., [Castillo, 2008](#); [Mazhari, 2016](#); [Wang et al., 2008](#)), and (II) magma mixing between a highly-enriched (OIB-like) and a relatively depleted (arc- or MORB-like) mantle source components ([Castillo, 2008](#); [Castillo et al., 2007](#); [Liu et al., 2017a, in press a](#)). The first model requires a young (<25 My old) oceanic crust subducted beneath the mantle wedge, and the presence of coeval adakite (e.g., [Castillo, 2008](#); [Mazhari, 2016](#); [Wang et al., 2008](#)), which is unlikely to be applicable to the Diancangshan-Ailaoshan case as no early Paleozoic adakite has ever been reported in the fold belt.

For the second model, [Cheng and Shen \(1997\)](#) reported continental rift-related alkaline metabasalts at Panjiazhai ([Fig. 1b](#)), which are OIB-like and were dated to be Early Silurian (ca. 430 Ma) ([Fig. 6](#); [Lai, 2012](#)). Thus, the enriched source of the Panjiazhai basaltic magma may have provided the enriched component for the mantle source mixing. Meanwhile, [Liu et al. \(2017b\)](#) reported that the Dalongkai gabbro in Ailaoshan was generated from an arc-like mantle source. Our simple magma source mixing model, using Panjiazhai metabasalt and

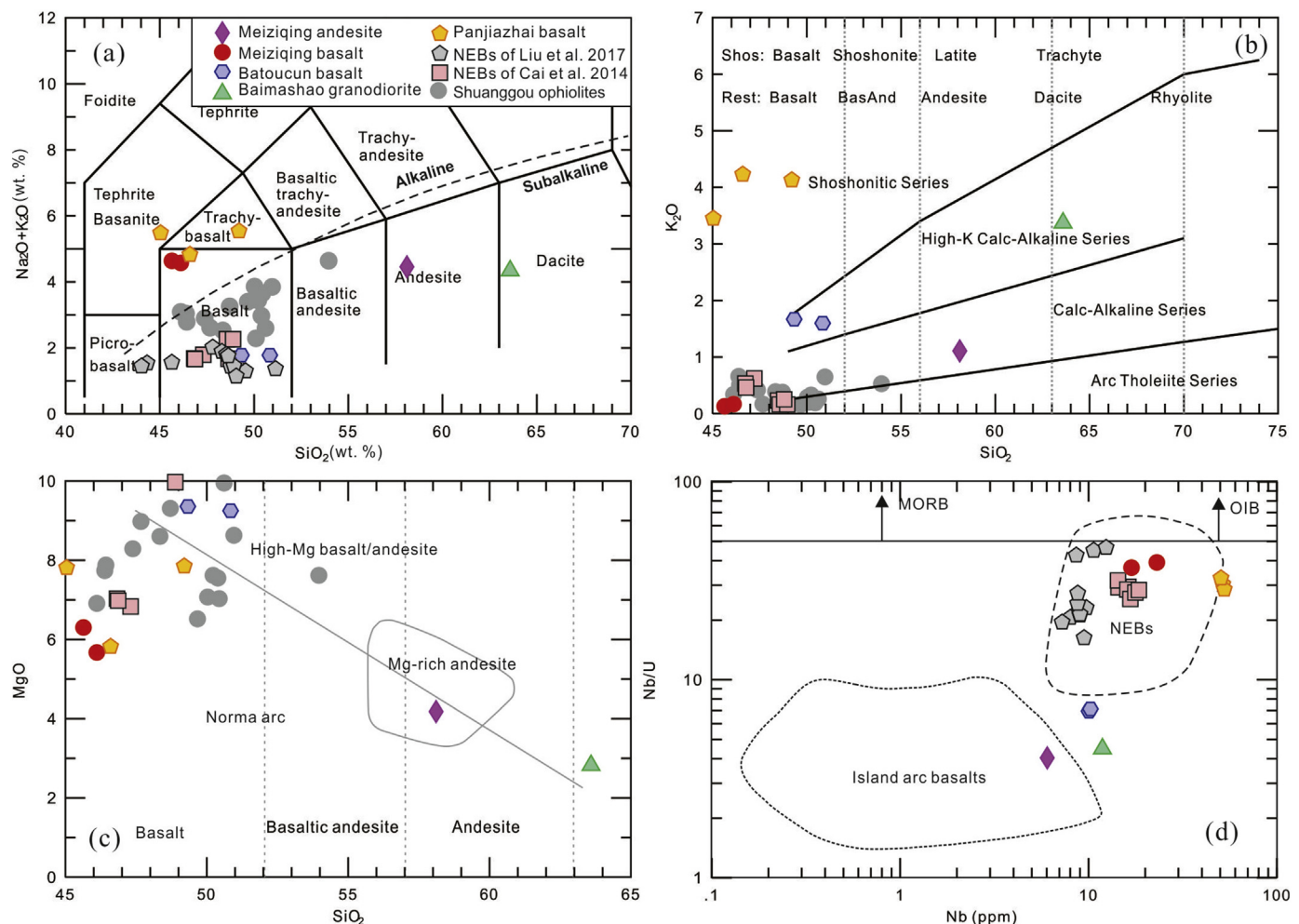


Fig. 5. Diagrams of (a) SiO₂ vs. K₂O + Na₂O (Le Bas et al., 1986); (b) K₂O vs. SiO₂ diagram (Le Maitre et al. 1989); (c) MgO vs. SiO₂; (d) Nb/U vs. Nb (Kepezhinskaya et al., 1996). NEBs: Nb-enriched basalts, HNBs: High-Nb basalts. The boundary between normal arc and high-Mg basalt/andesite, and the field of Mg-rich andesite are from Li et al. 2018 and references therein. Data of the Panjiazhai basalts (Cheng and Shen, 1997), NEBs from Liu et al. (2017b) and Cai et al. (2014), Ailaoshan ophiolites (Jian et al. 2009; Lai et al. 2014a, 2014b; Xu and Castillo, 2004) and Huimin arc volcanics (Xing et al., 2016 and Nie et al., 2015) were shown for comparison.

the Dalongkai gabbro as the two end-components, is illustrated in the binary plots of Nb versus various other incompatible trace elements (Fig. 8). The Meiziqing HNBs fall along the mixing lines, indicating that the mixing between an enriched OIB-like and a depleted arc-like mantle component could have generated the Meiziqing HNBs (Fig. 8). In the La vs. La/Yb and Nb vs. Yb diagrams, the Meiziqing HNBs and Panjiazhai metabasalts fall close to the garnet peridotite melting curves, similar to the Neoproterozoic Ailaoshan high-Nb amphibolite (Fig. 9; Cai et al., 2014). Compared with the Panjiazhai metabasalts, the Meiziqing HNBs were likely derived from a higher degree of partial melting of garnet peridotite (2% vs. 0.4%). The presence of garnet in the source region is also supported by the strong HREE depletions, which suggests that the melting occurred at a considerable depth (Xu et al., 2001). Hence, we propose that parental magmas of the Meiziqing HNBs were likely derived from the mixing between an enriched (OIB-like) and a depleted (arc-like) mantle components in the garnet stability field.

5.2. Formation of the Meiziqing Mg-rich andesite

The Meiziqing Mg-rich andesite is calc-alkaline (Figs. 5b and d) and contains negative $\varepsilon_{\text{Nd}}(t)$ values of -10.1 and negative Nb, Ta and Sr anomalies ($\text{Nb}^* = 0.14$; $\text{Sr}^* = 0.02$). This suggests that the Meiziqing andesite may not have formed from high-Nb, depleted ($\varepsilon_{\text{Nd}}(t) = +3.2$) alkali basaltic magma or from the mixing between crustal-derived and basaltic residual melts (which produces normal calc-alkaline

arc andesite) (Fig. 5d). The Meiziqing Mg-rich andesite shows low Sr/Y (0.28) and (La/Yb)_N (9.0) ratios and are not adakitic, which exclude an oceanic slab-melting origin. The Meiziqing Mg-rich andesite has negative $\varepsilon_{\text{Nd}}(t)$ values (-10.1), indicating crustal inputs in the magma source (e.g., Cai et al., 2014). Possible sources for these crustal components include sub-arc continental basement or subduction-derived sediments. Our magma source modeling suggests that around 10–15% South China continent crustal materials are required to achieve the observed Nd isotopic composition of the Meiziqing andesite (Fig. 10, e.g., Cai et al., 2014; Wang et al., 2013b). Such enormous volume of crustal materials in the mantle source is inconsistent with the incompatible element compositions and their ratios, and fails to account for the major oxide characteristics of the Meiziqing andesite. An alternative model for the Meiziqing andesite petrogenesis is that the andesite may have originated from a mixture of depleted mantle peridotite and melt from subducted sediment. Experimental studies have demonstrated that the melts become more siliceous as water content increases in the peridotitic source rocks (Kushiro, 1969; Hirose, 1997). Furthermore, melt compositions become more quartz-normative as pressure decreases (Mitchell & Grove, 2015). The medium-K, Mg-rich Yanhu andesites in southern Tibet (Li et al., 2018) can serve as an example for the andesite formed with its parental magma generated in shallow (~30 km deep) and H₂O-rich conditions, and we suggest that similar petrogenetic conditions were likely present for the parental magmas of the Meiziqing andesite.

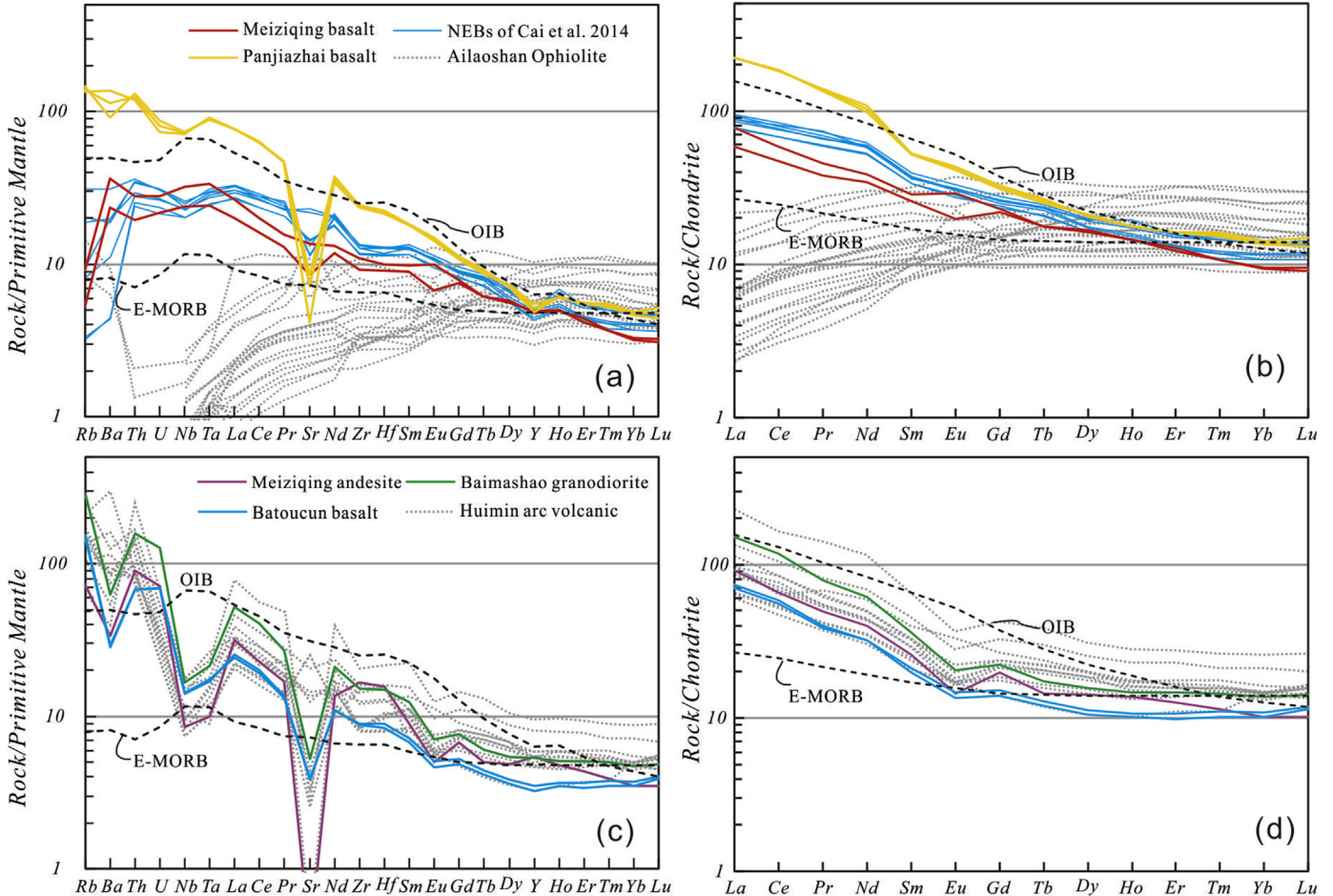


Fig. 6. (a and c) Primitive mantle-normalized multi-element spidergrams and (b and d) chondrite-normalized REE patterns for the HNBs and associated magmatic rocks in the Diancangshan-Ailaoshan fold belt. Normalizing values are from (Sun and McDonough, 1989). Data of the Panjiazhai basalts (Cheng and Shen, 1997), NEBs (Liu et al., 2014), Ailaoshan ophiolites (Jian et al. 2009; Lai et al. 2014a, 2014b; Xu and Castillo, 2004) and Huimin arc volcanics (Xing et al., 2016 and Nie et al., 2015) were shown for comparison.

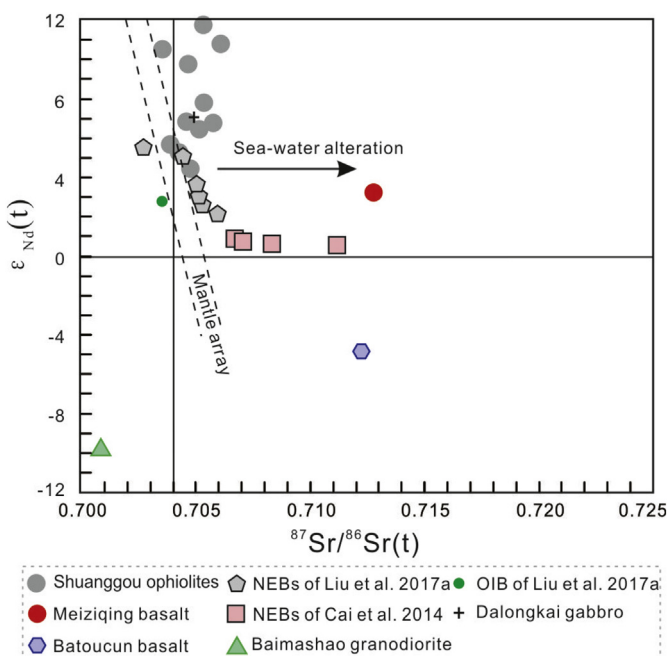


Fig. 7. $^{87}\text{Sr}/^{86}\text{Sr}$ (430 Ma) vs. ϵ_{Nd} (430 Ma) diagram. Data for the Jinshajiang and Shuanggou ophiolites are from Xu and Castillo (2004).

5.3. Formation of the Batoucun high-Mg basalt

Different models were proposed for the petrogenesis of the high-Mg basalts. For the high-Mg basalts in Kambalda (Western Australia), Arndt and Jenner (1986) and Sun and McDonough (1989) argued that they were the assimilation-fractional crystallization (AFC) products of the komatiitic magma, following the assimilation of large volumes of crustal material, whereas Cameron et al. (1979) and Redman and Keays (1985) proposed that they are the Archean analogs of modern boninite. Similarly, formation of the high-Mg basalts in the Bushveld Complex (South Africa) were also variably suggested to have been AFC-related (Sun and McDonough, 1989) or boninitic (Hamlyn and Keays, 1986). Peng et al. (2013) summarized these petrogenesis models into two groupds: (1) komatiite-derived and modified through crustal AFC processes, and (2) mafic equivalents of boninite, which are derived from the subduction-modified refractory continental lithospheric mantle.

No coeval komatiites have ever been reported along the Diancangshan-Ailaoshan fold belt, and thus we can preclude the komatiite-origin model. The high $\text{Mg}^{\#}$ values and Cr contents suggest that the Batoucun basalts can be considered to represent near-primary mantle melts (Mattioli et al., 2000). Their low HFSE abundances (e.g., $\text{Nb}^* = 0.30$) and enriched Sr-Nd isotopic composition ($^{87}\text{Sr}/^{86}\text{Sr}_i = 0.71224$ and $\epsilon_{\text{Nd}}(t) = -4.8$), indicate that their source region is enriched peridotitic mantle that has likely experienced one or more episodes of enrichment. Hence, their petrogenesis is likely comparable to that of typical boninite (e.g., Peng et al., 2013). The mantle source of

Table 3

Sr-Nd isotope compositions for the HNBs and associated magmatic rocks in the Diancangshan-Ailaoshan fold belt.

Sample	Age (Ga)	Rb/Sr	$^{87}\text{Rb}/^{86}\text{Sr}$	$^{87}\text{Sr}/^{86}\text{Sr}$	2 s	$(^{87}\text{Sr}/^{86}\text{Sr})_{\text{i}}$	$^{147}\text{Sm}/^{144}\text{Nd}$	$^{143}\text{Nd}/^{144}\text{Nd}$	2 s	$\epsilon_{\text{Nd}}(\text{t})$	$T_{\text{DM}}(\text{Ga})$	References
15YN-30B1	0.43	6.632	19.308	0.77062	17	0.65236	0.129	0.51193	9	-10.1	2.2	This study
15YN-30C1	0.43	0.019	0.054	0.71314	13	0.71281	0.150	0.51267	9	3.2	1.2	This study
15YN-35A	0.43	1.170	3.394	0.73303	15	0.71224	0.123	0.51218	8	-4.8	1.6	This study
15YN-65A	0.43	1.621	4.701	0.72969	13	0.70090	0.116	0.51191	10	-9.8	1.9	This study
10HH-67A	0.43	0.011	0.032	0.70691	13	0.70672	0.124	0.51248	8	0.8	1.2	Cai et al., 2014
10HH-67D	0.43	0.007	0.021	0.70723	13	0.70711	0.125	0.51248	6	0.8	1.2	Cai et al., 2014
10HH-69A	0.43	0.050	0.144	0.70924	12	0.70836	0.123	0.51246	8	0.6	1.2	Cai et al., 2014
10HH-69E	0.43	0.053	0.152	0.71217	12	0.71124	0.124	0.51246	8	0.5	1.2	Cai et al., 2014
10HH-22C	0.43	0.023	0.067	0.70489	11	0.70448	0.166	0.51281	8	5.0	1.1	Liu et al., 2017a
10HH-22E	0.43	0.163	0.471	0.70564	12	0.70276	0.161	0.51282	12	5.5	1.0	Liu et al., 2017a
10HH-22G	0.43	0.028	0.080	0.70542	9	0.70493	0.131	0.51281	6	7.0	0.6	Liu et al., 2017a
11ML-37A	0.43	0.005	0.015	0.70512	14	0.70503	0.181	0.51278	8	3.6	1.7	Liu et al., 2017a
11ML-37B	0.43	0.006	0.017	0.70601	17	0.70591	0.180	0.51270	7	2.1	2.1	Liu et al., 2017a
11ML-37E	0.43	0.004	0.012	0.70533	14	0.70526	0.183	0.51273	9	2.6	2.1	Liu et al., 2017a
11ML-37Z	0.43	0.001	0.004	0.70513	13	0.70510	0.180	0.51275	7	3.0	1.8	Liu et al., 2017a
EMI	0.43	0.100	0.289	0.70537	15	0.70360	0.170	0.51270	30	2.7	1.6	Liu et al., 2017b
97-002	0.43	0.032	0.092	0.70528		0.70472	0.257	0.51331		9.7	0.5	Xu and Castillo, 2004
97-002-pl	0.43	0.072	0.209	0.70662		0.70534	0.181	0.51319		11.7	-0.2	Xu and Castillo, 2004
97-002-1	0.43	0.005	0.014	0.70363		0.70355	0.223	0.51324		10.4	1.6	Xu and Castillo, 2004
97-003	0.43	0.020	0.058	0.70647		0.70611	0.209	0.51322		10.8	-2.1	Xu and Castillo, 2004
97-055-3	0.43	0.069	0.201	0.70590		0.70467	0.188	0.51296		6.8	1.1	Xu and Castillo, 2004
97-055-5	0.43	0.056	0.162	0.70638		0.70539	0.212	0.51308		7.7	8.5	Xu and Castillo, 2004
97-055-6	0.43	0.034	0.099	0.70644		0.70583	0.197	0.51298		6.7	1.5	Xu and Castillo, 2004
97-055-7	0.43	0.030	0.088	0.70575		0.70521	0.180	0.51292		6.4	1.1	Xu and Castillo, 2004
97-057	0.43	0.043	0.125	0.70550		0.70473	0.191	0.51285		4.4	2.1	Xu and Castillo, 2004
97-069-1	0.43	0.074	0.214	0.70559		0.70428	0.203	0.51292		5.1	3.3	Xu and Castillo, 2004
97-070	0.43	0.064	0.184	0.70509		0.70396	0.205	0.51295		5.6	3.6	Xu and Castillo, 2004

the Batoucun basalts may have been enriched mantle peridotite that was metasomatically enriched either by melts and/or hydrothermal fluids derived from the subducted oceanic crust and pelagic sediments prior to (or during) the remelting (e.g., Cervantes and Wallace, 2003; Mattioli et al., 2000; Melluso et al., 2006; Peng et al., 2013). It is noteworthy that the Batoucun basalts are characterized by enrichments of K₂O (1.6 to 1.7 wt%) and other highly incompatible elements (e.g., Th, U, and LREEs; Fig. 6). Recent geochemical studies from the Chilean Southern Volcanic Zone and global volcanic arcs indicate that arc compositional variability (e.g., K₂O) is mainly controlled by varying degree of partial melting of the mantle wedge, in response to the different thermal structure of the latter (Turner et al., 2016). The Batoucun high-K basalts have relatively low $\epsilon_{\text{Nd}}(\text{t})$ values (-4.8), implying the involvement of pelagic sediments in the mantle source. Thus, the Batoucun high-Mg basalts were likely derived from the partial melting of an enriched mantle metasomatized by subduction-related, pelagic sediment-derived fluids.

5.4. Formation of the Baimashao I-type granite

The Baimashao granodiorite is high-K I-type, which could be formed via: (1) fractional crystallization of mantle-derived basaltic magma (Barth et al., 1995) or (2) partial melting of sub-alkaline meta-basalts, followed by fractionation (Rapp and Watson, 1995). In the Diancangshan-Ailaoshan fold belt, potential magma sources for the Baimashao granodiorite may have been the coeval Meiziqing HNB, Meiziqing andesite and the Batoucun basalt. Among these three potential sources, the Meiziqing HNB and Batoucun basalt show much higher $\epsilon_{\text{Nd}}(\text{t})$ values than the Baimashao I-type granites (+3.2, -4.8 and -9.8, respectively). Since large volume of mafic magma is needed to produce (fractionate) small amount of silicic rocks (Peccerillo et al., 2003), yet (apart from the Meiziqing HNB and andesite, and Batoucun basalt) there are few other Ordovician-Silurian mafic rocks reported in the region, we propose that fractional crystallization of mafic magma was unlikely to be the main petrogenetic mechanism for the Baimashao granodiorite. Experimental studies suggest that intermediate to felsic melts can be produced by dehydration melting of meta-basaltic rocks, leaving behind a granulite residue (at 8–12 kbar) or a garnet granulite

to eclogite residue (at 12–32 kbar) (Rapp and Watson, 1995), which we consider to be more plausible for the formation of the Baimashao granodiorite.

6. Tectonic implications for the South China break-away from Gondwana

6.1. Early Paleozoic intracontinental back-arc rifting in the Diancangshan-Ailaoshan region

HNBs and OIB-like basalts are considered to have formed under local/regional extension caused by slab rollback or subduction-unrelated lithospheric delamination (Castillo, 2008, 2009; Castillo et al., 2007, 2002; Liu et al., 2017a; Straub et al., 2013). In the Diancangshan-Ailaoshan fold belt, no evidence for an early Paleozoic lithospheric delamination has been reported. The Silurian Diancangshan-Ailaoshan mafic rocks contain high Zr contents and high Zr/Y, Nb/Y and Ti/Y ratios, and fall into the within-plate basalt field in various tectonic discrimination diagrams (Fig. 11). We considered that these within-plate characters were formed by slab rollback-induced regional extension because: (1) Most high-Nb mafic rocks are oceanic subduction-related, no matter they are adakitic or OIB-like (e.g., Aguilera-Robles et al., 2001; Azizi et al., 2014; Castillo, 2009; Hastie et al., 2011; Imaoka et al., 2017; Liu et al., 2017a; Macpherson et al., 2010; Mazhari, 2016; Petrone and Ferrari, 2008; Wang et al., 2008; 2007b); (2) The Diancangshan-Ailaoshan high-Mg basalts show distinct negative Nb-Ta and Sr anomalies and plot in the arc basalt field (Figs. 11b and d). They also have high Zr, Ta, La contents and high Zr/Y ratios, and fall into the within-plate basalt field (Figs. 11a, c-d). This coexistence of arc and within-plate affinities were also reported in the high-Mg basalts from, e.g., southern Sardinia (Italy; Mattioli et al., 2000), Chichinautzin in central Mexico (Cervantes and Wallace, 2003), and the Deccan Traps (India; Melluso et al., 2006); (3) The Meiziqing Mg-rich andesite show typical arc signatures (Fig. 6c); (4) The Baimashao granodiorite was likely to have formed in a continental arc setting, since no coeval (post)-collisional events were reported. In summary, we suggest that the Late Ordovician-Silurian Diancangshan-Ailaoshan tectonics was controlled by the slab rollback-induced

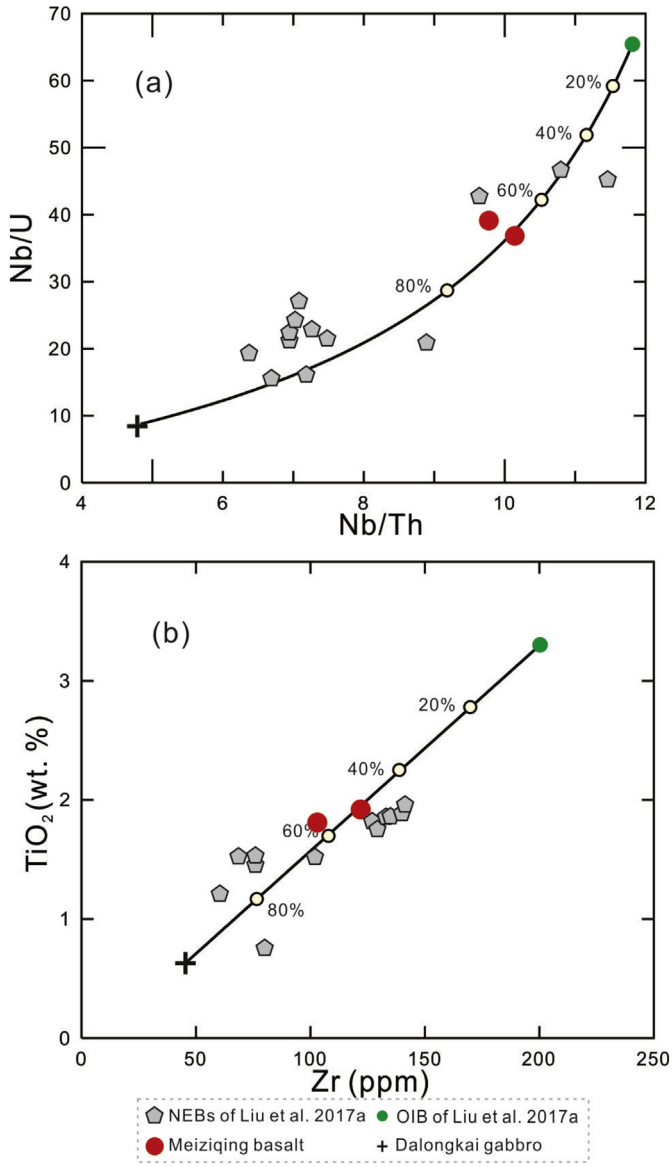


Fig. 8. Diagrams of (a) Nb/Th vs. Nb/U and (c) Zr vs. TiO₂. Also shown are model mixing between the OIB-like and arc-like mantle components. Tick symbols in the curves denote the amount of arc-like component in the mixture. The Panjiazhai metabasalt and the Dalongkai gabbro represent the two OIB-like and arc-like end components.

extension. The consequent asthenosphere upwelling likely provided sufficient heat to trigger the partial melting of the ancient enriched mantle and the sub-alkaline meta-basalts, which produced the Meiziqing HNB and Mg-rich andesite, Batoucun high-Mg basalt, and the Baimashao granodiorite (Fig. 12).

6.2. Protethyan subduction and break-away of South China from Gondwana

During the early Paleozoic, the Simao-Indochina, Lhasa, Sibumasu and South China block may have constituted the northern Gondwana passive margin (Brookfield, 1993; Zhu et al., 2015; Miller et al., 2001), and various studies suggested that subduction-related magmatism may have started from the late Cambrian (ca. 492 Ma; Wang et al., 2013c). These magmatic rocks include the Ordovician-Silurian SSZ-type ophiolites at Nantinghe (ca. 473–444 Ma) and Tongchangjie (ca. 444–439 Ma) Wang et al. (2013a), the Huimin arc-type mafic-intermediate volcanic rocks (ca. 462–454 Ma) (Figs. 6c-d; Nie et al., 2015; Xing et al., 2016), and the continental back-arc basin-related Dazhonghe and

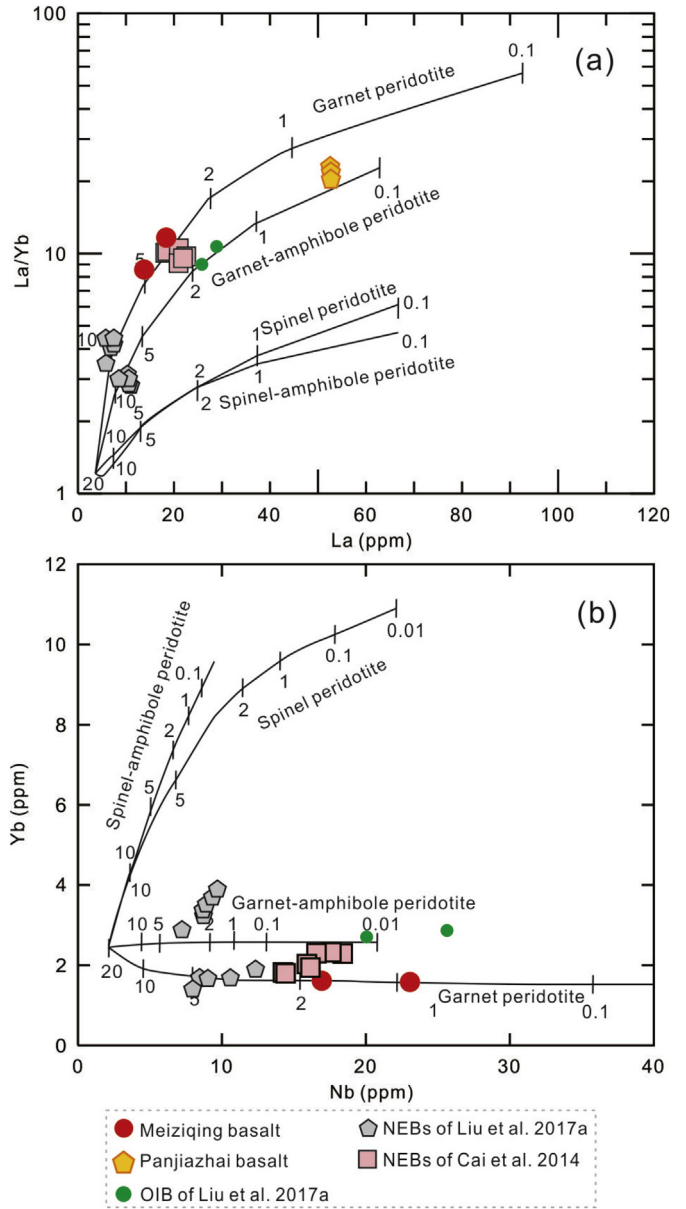


Fig. 9. Diagrams of (a) La vs. La/Yb, (b) Nb vs. Yb, which model the partial melting of the different mantle sources (Imaoka et al., 2014; Zhang et al., 2006). The grid indicates the range of model compositions. The proportion of melt formed in the presence of garnet is indicated by the numbers in %.

Dawazi volcanic rocks (ca. 420 Ma) (Liu et al., in press b; Lehmann et al., 2013). High-pressure greenschist from the upper part of the Lancang Group were $^{40}\text{Ar}/^{39}\text{Ar}$ dated to be ~410 Ma, and may have had an igneous protolith (Cong et al., 1993). The distribution of these ophiolites and arc-related rocks indicate the east-dipping (present orientation) of the Protethys in the region (Figs. 1 and 12a).

After the amalgamation of the South China and Simao-Indochina blocks in the Neoproterozoic (ca. 860–730 Ma; Cai et al., 2014, 2015; Qi et al., 2012, 2014; Wang et al., 2016), the Diancangshan-Ailaoshan region has likely experienced long magmatic quiescence. Jian et al. (2009) reported the presence of Silurian low-Ti CFB (continental flood basalt; ca. 443–401 Ma) in the northern Jinshajiang region. Low-Ti CFB is commonly produced by partial melting of hydrated, depleted peridotite in the lithospheric mantle during incipient continental rifting (Jolly, 1987). Besides, the Dawazi Formation (ca. 420 Ma) is also marked by continental rift-related bimodal volcanic rocks, abyssal-bathyal spilite-keratophyre and flysch sequences (Li, 2012; Liu et al., in press b). The

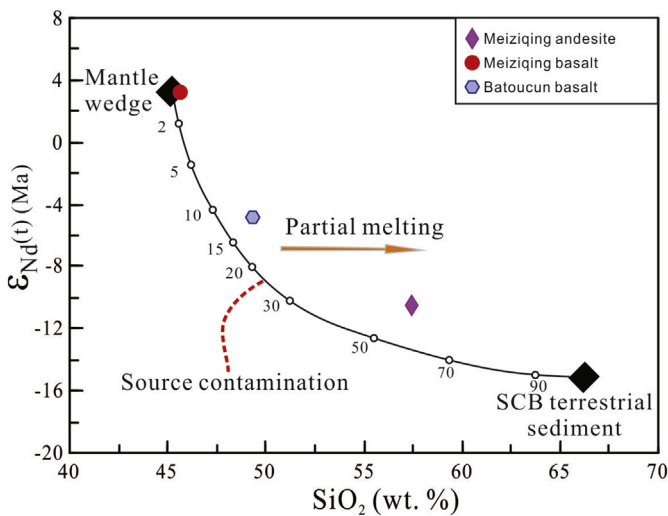


Fig. 10. Plots of SiO_2 versus $\varepsilon_{\text{Nd}}(t)$ (Wang et al., 2013b). The black solid line denotes source contamination of the mantle wedge with SCC crustal sediment. The mantle wedge is characterized by $\text{SiO}_2 = 45 \text{ wt\%}$, $\text{Nd} = 4.5 \text{ ppm}$, $\text{Sr} = 60 \text{ ppm}$, $^{87}\text{Sr}/^{86}\text{Sr}(t) = 0.7030$ and $\varepsilon_{\text{Nd}}(t) = +3.0$. SCB crust sediment has $\text{SiO}_2 = 66 \text{ wt\%}$, $\text{Nd} = 26.3 \text{ ppm}$, $\text{Sr} = 206 \text{ ppm}$, $^{87}\text{Sr}/^{86}\text{Sr}(t) = 0.7130$, and $\varepsilon_{\text{Nd}}(t) = -15.0$.

Upper Silurian radiolarian chert in the Dapingzhang Cu deposit (Li, 2012), and the coeval neritic bioclastic limestone, intramicrite, graptolite shale and quartz sandstone from the Changdu basin west of

Diancangshan (Du et al., 1997) indicate that the continental rift may have developed into an ocean basin by the late Silurian. These, together with the Diancangshan-Ailaoshan rocks presented in this study, suggest an intracontinental back-arc rift setting for the Late Ordovician-Silurian SW Yunnan. In other words, South China may have commenced its break-up from Gondwana from the Late Ordovician (ca. 446 Ma). This conclusion is also consistent with our published sedimentological and detrital zircon U-Pb and Lu-Hf isotope data on the Cambrian-Devonian sedimentary units in the Ailaoshan fold belt and its adjacent western South China margin (Xia et al., 2016). The changes in regional sedimentary facies from Silurian-Lower Devonian siliciclastic rocks to Upper Devonian-Carboniferous pelagic rocks (shale, limestone and chert) suggest that the continental rift may have developed into a wide ocean by Carboniferous (Xia et al., 2016), as also demonstrated by the extensive occurrences of ophiolites. We thereby summarize the break-away of South China and the Paleotethys opening into several stages, including (I) tectonic (non-volcanic) rifting (ca. 446–401 Ma), (II) main-stage seafloor spreading (ca. 387–377 Ma), (III) rifting with asthenospheric upwelling (ca. 359–345 Ma), and (IV) late-phase seafloor spreading (ca. 346–265 Ma; Jian et al., 2009; Lai et al., 2014a, 2014b; Zhang et al., 2013, 2014; Zi et al., 2012; Liu et al., 2018). After reaching its maximum expansion during the Late Carboniferous, the back-arc basin may have started to close by subducting westward beneath the Simao-Indochina block, and generated the Late Carboniferous-Permian Jomda-Weixi (Yang et al., 2014), Wusu-Yaxuanqiao (Fan et al., 2010), Truong Son (Kamvong et al., 2014; Liu et al., 2012; Shi et al., 2015), Jianshui (Dong and Zhu 1999) and Cao Bang (Halpin et al., 2016;

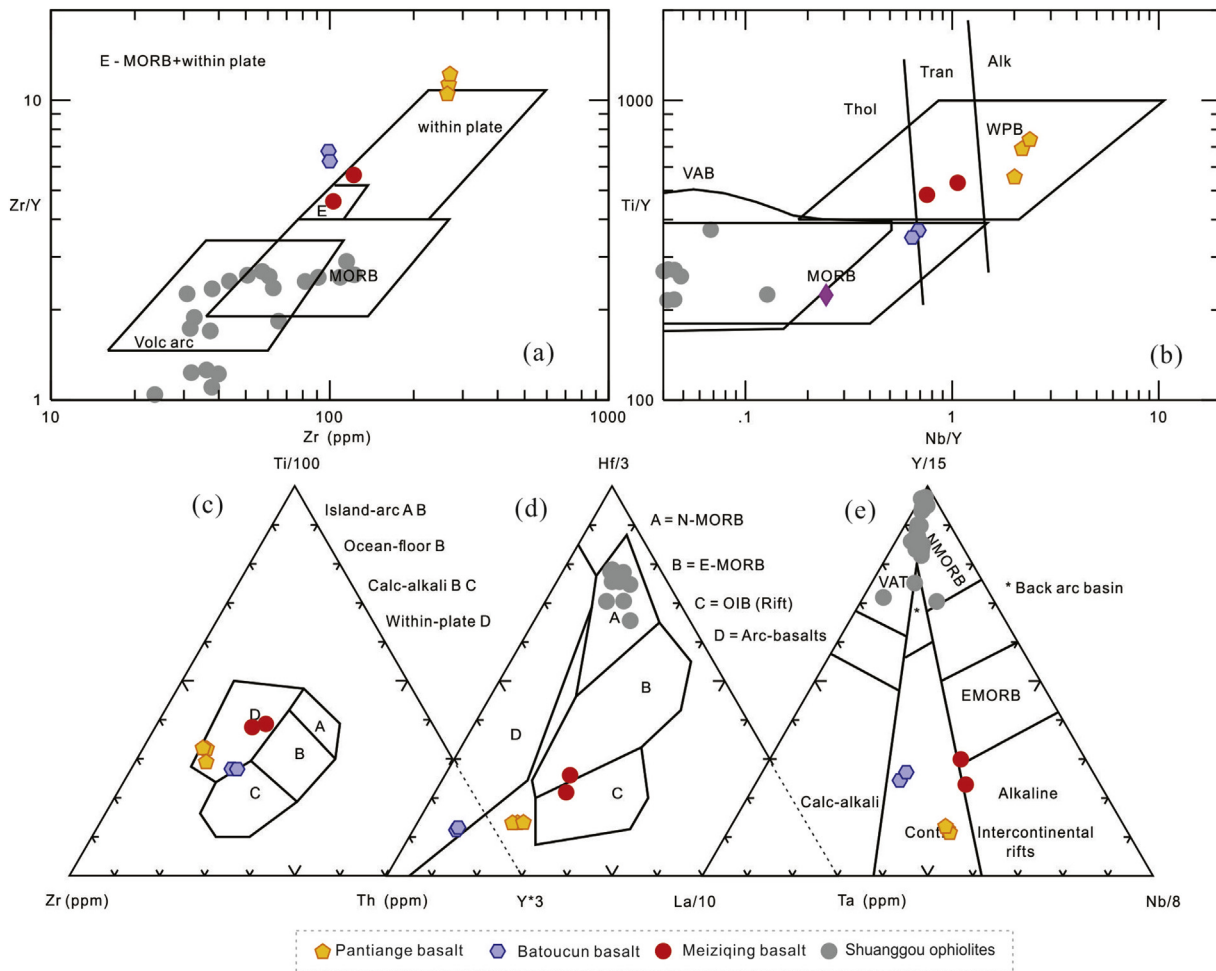


Fig. 11. Tectonic discrimination diagrams for the Meiletu, Batoucun and Panjiazhai basalts: (a) Zr vs. Zr/Y , (b) Nb/Y vs. Ti/Y , (c) $\text{Ti}/100-\text{Zr}-\text{Y}^*3$, (d) $\text{Hf}/3-\text{Th}-\text{Ta}$ and (e) $\text{Y}/15-\text{La}/10-\text{Nb}/8$.

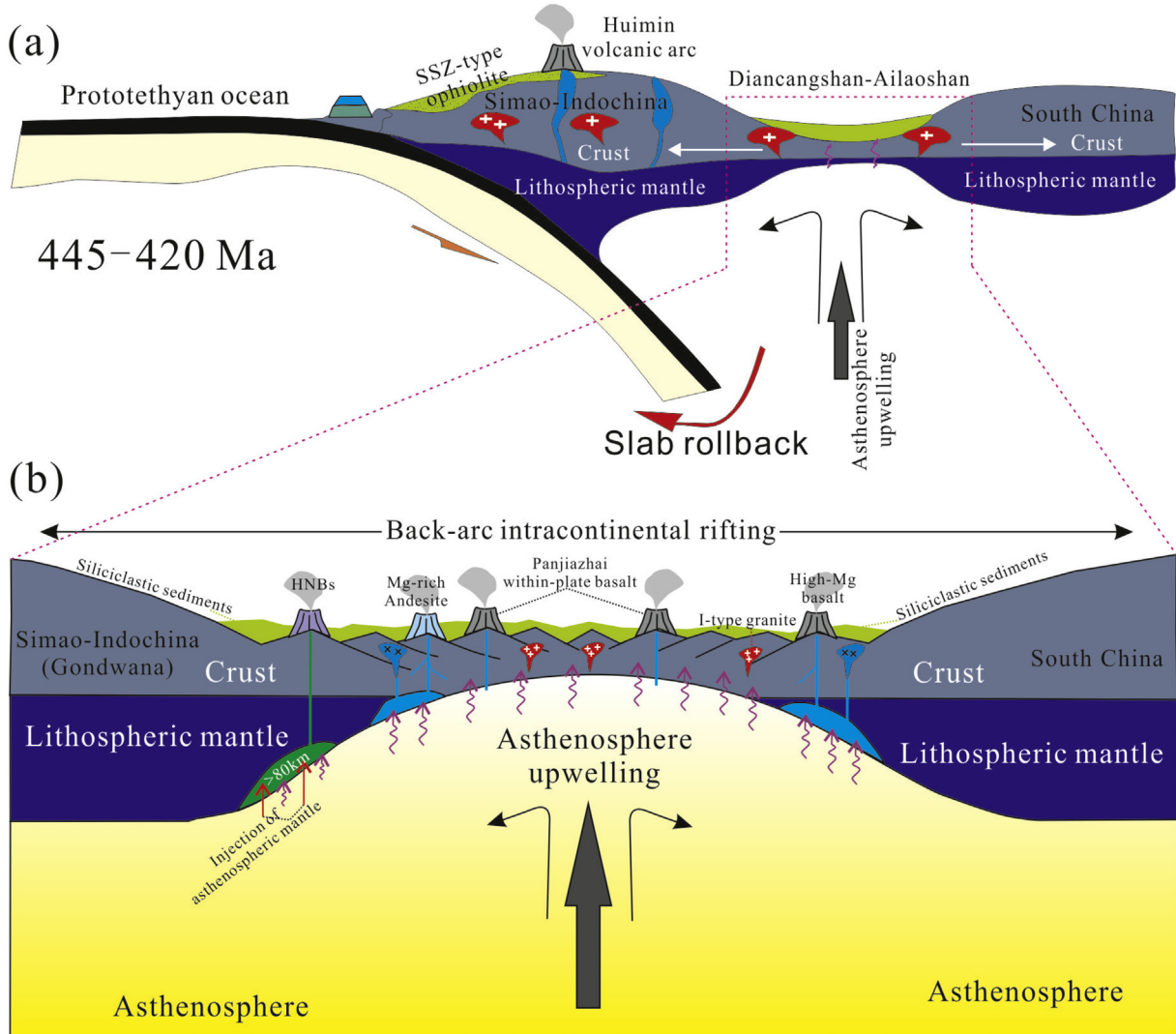


Fig. 12. Schematic tectonic diagram showing the Ordovician-Silurian slab rollback and intracontinental back-arc rifting of the South China from the Gondwana. The asthenosphere upwelling provided sufficient heat to trigger the partial melting of the garnet peridotite, the ancient enriched mantle and the sub-alkaline meta-basalts, which produced the Silurian Meiziqing HNB and Mg-rich andesite, Batoucun high-Mg basalt, and Baimashao granodiorite.

Thanh et al., 2014) arc/back-arc basin magmatic rocks in the Jinshajiang, Ailaoshan and Song Ma fold belts, respectively.

7. Conclusions

(1) Silurian high-Nb basalt (HNB), Mg-rich andesite, high-Mg basalt and granodiorite were formed in the Late Ordovician-Silurian (ca. 446–420 Ma) along the Diancangshan-Ailaoshan fold belt.

(2) The HNBs were likely derived from the mixing between an enriched OIB-like and a depleted arc-like mantle source in the garnet stability field. The Mg-rich andesite was generated by partial melting of depleted mantle peridotites metasomatized by subducted sediment melts under low pressure and H_2O -rich conditions. The high-Mg basalt was derived from an enriched mantle source metasomatized by subduction-related, pelagic sediment-derived fluids. The granodiorite was likely from the partial melting of meta-basalts.

(3) The Diancangshan-Ailaoshan HNB, Mg-rich andesite, high-Mg basalt and granodiorite may have formed in an intracontinental back-arc rift setting.

(4) South China may have commenced its break-up from Gondwana in the Late Ordovician (ca. 446 Ma), in response to the east-dipping

(modern orientation) subduction of the Prototethys and the subsequent opening of the Ailaoshan back-arc ocean basin.

Acknowledgments

This study is financially supported by the National Natural Science Foundation of China (41502210 and 41704091). We would like to thank Drs. X. F. Guo, Q.-L. Tan, S.-B. Li, L.-M. Zhang and H.-Y. He for helping with the field work and zircon U-Pb analyses. The editor and two anonymous reviewers are thanked for their constructive comments and suggestions.

Appendix A. Supplementary data

Supplementary data to this article can be found online at <https://doi.org/10.1016/j.lithos.2018.08.014>.

References

- Aguillon-Robles, A., Calmus, T., Benoit, M., Bellon, H., Maury, R.O., Cotten, J., Bourgois, J., Michaud, F., 2001. Late miocene adakites and Nb-enriched basalts from Vizcaino peninsula, Mexico: indicators of East Pacific rise subduction below southern Baja California? *Geology* 29 (6), 531–534.

- Arndt, N.T., Jenner, G.A., 1986. Crustally contaminated komatiites and basalts from Kambalda, Western Australia. *Chemical Geology* 56, 229–255.
- Azizi, H., Asahara, Y., Tsuboi, M., 2014. Quaternary high-Nb basalts: existence of young oceanic crust under the Sanandaj-Sirjan zone, NW Iran. *International Geology Review* 56 (2), 167–186.
- Barth, A.P., Wooden, J.L., Tosdal, R.M., Morrison, J., 1995. Crustal contamination in the Petrogenesis of a Calc-Alkaline rock series - Josephine Mountain intrusion, California. *Geological Society of America Bulletin* 107 (2), 201–212.
- Brookfield, M.E., 1993. The Himalaya passive margin from Precambrian to cretaceous times. *Sedimentary Geology* 84, 1–35.
- Buitler, S.J.H., Torsvik, T.H., 2014. A review of Wilson cycle plate margins: a role for mantle plumes in continental break-up along sutures? *Gondwana Research* 26 (2), 627–653.
- Burrett, C., Zaw, K., Meffre, S., Lai, C.K., Khositanont, S., Chaodumrong, P., Udhachon, M., Ekins, S., Halpin, J., 2014. The configuration of greater Gondwana-evidence from LA ICPMS, U-Pb geochronology of detrital zircons from the Palaeozoic and Mesozoic of Southeast Asia and China. *Gondwana Research* 26 (1), 31–51.
- Cai, Y.F., Wang, Y.J., Cawood, P.A., Fan, W.M., Liu, H.C., Xing, X.W., Zhang, Y.Z., 2014. Neoproterozoic subduction along the Ailaoshan zone, South China: Geochronological and geochemical evidence from amphibolite. *Precambrian Research* 245 (5), 13–28.
- Cai, Y.F., Wang, Y.J., Cawood, P.A., Zhang, Y.Z., Zhang, A.M., 2015. Neoproterozoic crustal growth of the southern Yangtze block: geochemical and zircon U-Pb geochronological and Lu-Hf isotopic evidence of Neoproterozoic diorite from the Ailaoshan zone. *Precambrian Research* 266, 137–149.
- Cameron, W.E., Nisbet, E.G., Dietrich, V.J., 1979. Boninites, komatiites and ophiolitic basalts. *Nature* 280, 550–553.
- Castillo, P.R., 2008. Origin of the adakite-high-Nb basalt association and its implications for postsubduction magmatism in Baja California, Mexico. *Geological Society of America Bulletin* 120 (3–4), 451–462.
- Castillo, P.R., 2009. Origin of Nb-enriched basalts and adakites in Baja California, Mexico, revisited: reply. *Geological Society of America Bulletin* 121 (9–10), 1470–1472.
- Castillo, P.R., Solidum, R.U., Punongbayan, R.S., 2002. Origin of high field strength element enrichment in the Sulu arc, southern Philippines, revisited. *Geology* 30 (8), 707–710.
- Castillo, P.R., Rigby, S.J., Solidum, R.U., 2007. Origin of high field strength element enrichment in volcanic arcs: geochemical evidence from the Sulu arc, southern Philippines. *Lithos* 97 (3–4), 271–288.
- Cervantes, P., Wallace, P.J., 2003. Role of H₂O in subduction-zone magmatism: new insights from melt inclusions in high-mg basalts from Central Mexico. *Geology* 31 (3), 235–238.
- Chappell, B.W., White, A.J.R., 1992. I-type and S-type granites in the Lachlan tectonic zone. *Transactions of the Royal Society of Edinburgh-Earth Sciences* 83 (83), 1–26.
- Cheng, H.L., Shen, S.Y., 1997. Metamorphic basalts in Panjiazhai, Aila Mountain area, Yunnan. *Tethyan Geology* (in Chinese with English abstract) 21, 62–72.
- Cong, B.L., Wu, G.Y., Zhang, Q., Zhang, R.Y., Zhai, M.G., Zhao, D.S., Zhang, W.H., 1993. Petrotectonic evolution of the Tethys zone in western Yunnan, China. *Science in China (series B)* 23, 1201–1207 in Chinese.
- Deng, J., Wang, Q.F., Li, G.J., Santosh, M., 2014. Cenozoic tectono-magmatic and metallogenetic processes in the Sanjiang region, southwestern China. *Earth-Science Reviews* 138, 268–299.
- Dong, Y.P., Zhu, B.Q., 1999. Geochemical characteristics of the arc basalts in Jianshui area (SE Yunnan province) and its tectonic implication for the Paleotethyan evolution in SW China. *Chinese Science Bulletin* 44, 2323–2327 (In Chinese).
- Du, D.X., Luo, J.N., Li, X.Z., 1997. Sedimentary evolution and palaeogeography of the Qamdo block in Tibet. *Lithofacies and Paleogeography* 17, 1–17 in Chinese with English abstract.
- Fan, W.M., Wang, Y.J., Zhang, A.M., Zhang, F.F., Zhang, Y.Z., 2010. Permian arc-back-arc basin development along the Ailaoshan tectonic zone: geochemical, isotopic and geochronological evidence from the Mojiang volcanic rocks, Southwest China. *Lithos* 119 (3–4), 553–568.
- Halpin, A.J., Tran, T.H., Lai, C.K., Meffre, S., Crawford, A.J., Zaw, K., 2016. U-Pb zircon geochronology and geochemistry from NE Vietnam: A 'tectonically disputed' territory between the Indochina and South China blocks. *Gondwana Research* 34 (2016), 254–273.
- Hamlyn, P.R., Keays, R.R., 1986. Sulfur saturation and second stage melts: applications to the Bushveld platinum metal deposits. *Economic Geology and the Bulletin of the Society of Economic Geologists* 81, 1431–1445.
- Hanchar, J.M., Miller, C.F., 1993. Zircon zonation patterns as revealed by cathodoluminescence and backscattered electron images - implications for interpretation of complex crustal histories. *Chemical Geology* 110 (1–3), 1–13.
- Hastie, A.R., Mitchell, S.F., Kerr, A.C., Minifie, M.J., Millar, I.L., 2011. Geochemistry of rare high-Nb basalt lavas: are they derived from a mantle wedge metasomatised by slab melts? *Geochimica et Cosmochimica Acta* 75 (17), 5049–5072.
- Hirose, K., 1997. Melting experiments on Iherzolite KLB-1 under hydrous conditions and generation of high-magnesian andesitic melts. *Geology* 25 (1), 42–44.
- Imaoka, T., Nakashima, K., Kamei, A., Itaya, T., Ohira, T., Nagashima, M., Kono, N., Kiji, M., 2014. Episodic magmatism at 105 ma in the Kinki district, SW Japan: petrogenesis of Nb-rich lamprophyres and adakites, and geodynamic implications. *Lithos* 184–187, 105–131.
- Imaoka, T., Kawabata, H., Nagashima, M., Nakashima, K., Kamei, A., Yagi, K., Itaya, T., Kiji, M., 2017. Petrogenesis of an early cretaceous lamprophyre dike from Kyoto prefecture, Japan: implications for the generation of high-Nb basalt magmas in subduction zones. *Lithos* 290, 18–33.
- Jian, P., Liu, D.Y., 2002. U-Pb zircon dating of the Caledonian Gongbo gabbro from the Mid-Jinshajiang area, Sichuan province. *Geological Review* 48 (SI), 17–22.
- Jian, P., Liu, D.Y., Kroner, A., Zhang, Q., Wang, Y.Z., Sun, X.M., Zhang, W., 2009. Devonian to Permian plate tectonic cycle of the paleo-Tethys Orogen in Southwest China (II): insights from zircon ages of ophiolites, arc/back-arc assemblages and within-plate igneous rocks and generation of the Emeishan CFB province. *Lithos* 113 (3–4), 767–784.
- Jolly, W.T., 1987. Lithophile elements in Huronian low-Ti continental tholeites from Canada, and evolution of the Precambrian mantle. *Earth and Planetary Science Letters* 85, 401–417.
- Kamvong, T., Zaw, K., Meffre, S., Maas, R., Stein, H., Lai, C.K., 2014. Adakites in the Truong son and Loei tectonic zones, Thailand and Laos: genesis and implications for geodynamics and metallogeny. *Gondwana Research* 26, 165–184.
- Kemp, A.I.S., Whitehouse, M.J., Hawkesworth, C.J., Alarcon, M.K., 2005. A zircon U-Pb study of metaluminous (I-type) granites of the Lachlan Tectonic zone, southeastern Australia: implications for the high/low temperature classification and magma differentiation processes. *Contributions to Mineralogy and Petrology* 150 (2), 230–249.
- Kepezhinskis, P., Defant, M.J., Drummond, M.S., 1996. Progressive enrichment of island arc mantle by melt-peridotite interaction inferred from Kamchatka xenoliths. *Geochimica et Cosmochimica Acta* 60 (7), 1217–1229.
- Kushiro, I., 1969. The system forsterite-diopside-silica with and without water at high pressures. *American Journal of Science* 267, 269–294.
- Lai, C.K., 2012. Tectonic Evolution of the Ailaoshan Tectonic Zone in SW Yunnan, China. *ARC Centre of Excellence in Ore Deposits (CODES)*, University of Tasmania, Hobart.
- Lai, C.K., Meffre, S., Crawford, A.J., Zaw, K., Halpin, J.A., Xue, C.D., Salam, A., 2014a. The central Ailaoshan ophiolite and modern analogs. *Gondwana Research* 26 (1), 75–88.
- Lai, C.K., Meffre, S., Crawford, A.J., Zaw, K., Xue, C.D., Halpin, J.A., 2014b. The western Ailaoshan volcanic belts and their SE Asia connection: a new tectonic model for the eastern Indo-China block. *Gondwana Research* 26 (1), 52–74.
- Le Bas, M.J., Le Maitre, R.W., Streckeisen, A., Zanettin, B., 1986. A chemical classification of volcanic rocks based on the total alkali-silica diagram. *Journal of Petrology* 27, 745–750.
- Le Maitre, R.W., Bateman, P., Dudek Keller, A.J., Lameyre Le Bas, M.J., Sabine, P.A., Schmid, R., Sorensen, H., Streckeisen, A., Wolley, A.R., Zanettin, B., 1989. A classification of igneous rocks and glossary of terms. Blackwell, Oxford, pp. 193–198.
- Lehmann, B., Zhao, X.F., Zhou, M.F., Du, A.D., Mao, J.W., Zeng, P.S., Henjes-Kunst, F., Heppe, K., 2013. Mid-Silurian back-arc spreading at the northeastern margin of Gondwana: the Dapingzhang dacite-hosted massive sulfide deposit, Lancangjiang zone, southwestern Yunnan, China. *Gondwana Research* 24 (2), 648–663.
- Li, J.B., 2012. Geochemical characteristics of the volcanic rocks in Dapingzhang copper deposit (China). Master's Thesis of Kunming University of Science and Technology, pp. 1–80 (In Chinese with English abstract).
- Li, Q.L., Li, X.H., Wu, F.Y., Yin, Q.Z., Ye, H.M., Liu, Y., Tang, G.Q., Zhang, C.L., 2012. In-situ SIMS U-Pb dating of phanerozoic apatite with low U and high common Pb. *Gondwana Research* 21 (4), 745–756.
- Li, S.M., Wang, Q., Zhu, D.C., Stern, C.R., Cawood, P., Sui, Q.L., Zhao, Z.D., 2018. One or two early cretaceous arc systems in the Lhasa Terrane, southern Tibet. *Journal of Geophysical Research: Solid Earth* 123 (5), 3391–3413.
- Liu, Y.S., Hu, Z.C., Gao, S., Gunther, D., Xu, J., Gao, C.G., Chen, H.H., 2008. In situ analysis of major and trace elements of anhydrous minerals by LA-ICP-MS without applying an internal standard. *Chemical Geology* 257 (1–2), 34–43.
- Liu, J.L., Tran, M.D., Tang, Y., Nguyen, Q.L., Tran, T.H., Wu, W.B., Chen, J.F., Zhang, Z.C., Zhao, Z.D., 2012. Permo-Triassic granitoids in the northern part of the Truong son belt, NW Vietnam: geochronology, geochemistry and tectonic implications. *Gondwana Research* 22, 628–644.
- Liu, H.C., Wang, Y.J., Fan, W.M., Zi, J.W., Cai, Y.F., Yang, G.L., 2014. Petrogenesis and tectonic implications of late-Triassic high E > (Nd)(t)-E > (Hf)(t) granites in the Ailaoshan tectonic zone (SW China). *Science China-Earth Sciences* 57 (9), 2181–2194.
- Liu, H.C., Wang, Y.J., Cawood, P.A., Guo, X.F., 2017a. Episodic slab rollback and back-arc extension in the Yunnan-Burma region: insights from cretaceous Nb-enriched and oceanic-island basalt-like mafic rocks. *Geological Society of America Bulletin* 129 (5–6), 698–714.
- Liu, H.C., Wang, Y.J., Zi, J.W., 2017b. Petrogenesis of the Dalongkai ultramafic-mafic intrusion and its tectonic implication for the Paleotethyan evolution along the Ailaoshan tectonic zone (SW China). *Journal of Asian Earth Sciences* 141 (2017), 112–124.
- Liu, H.C., Peng, T.P., Guo, X.F., 2018. Geochronological and geochemical constraints on the coexisting N-MORB- and SSZ-type ophiolites in Babu area (SW China) and tectonic implications. *Journal of the Geological Society* 175 (3), 1–12.
- Liu, H.C., Li, Y.L., Wu, L.W., Huangfu, P.P., Zhang, M., in press a. Geochemistry of high-Nb basalt-andesite in the Erguna Massif (NE China) and implications for the early Cretaceous back-arc extension. *Geological Journal* 1–17 <https://doi.org/10.1002/gj.3176>.
- Liu, H.C., Bi, M.W., Guo, X.F., Zhou, Y.Z., Wang, Y.K., in press b. Petrogenesis of late Silurian volcanism in SW Yunnan (China) and implications for the tectonic reconstruction of northern Gondwana. *International Geology Review*, <https://doi.org/10.1080/00206814.2018.1506947>.
- Macpherson, C.G., Chiang, K.K., Hall, R., Nowell, G.M., Castillo, P.R., Thirlwall, M.F., 2010. Plio-Pleistocene intra-plate magmatism from the southern Sulu arc, Semporna peninsula, Sabah, Borneo: implications for high-Nb basalt in subduction zones. *Journal of Volcanology and Geothermal Research* 190 (1–2), 25–38.
- Mao, X.C., Wang, L.Q., Li, B., Wang, B.D., Wang, D.B., Yin, F.G., Sun, Z.M., 2012. Discovery of the late Silurian volcanic rocks in the Dazhonghe area, Yunxian-Jinggu volcanic arc belt, western Yunnan, China and its geological significance. *Acta Petrologica Sinica* 28, 1517–1528 (In Chinese with English abstract).
- Mattioli, M., Guerrera, F., Tramontana, M., Raffaelli, G., D'Atri, M., 2000. High-Mg tertiary basalts in southern Sardinia (Italy). *Earth and Planetary Science Letters* 179 (1), 1–7.
- Mazhari, S.A., 2016. Petrogenesis of adakite and high-Nb basalt association in the SW of Sabzevar zone, NE of Iran: evidence for slab melt-mantle interaction. *Journal of African Earth Sciences* 116, 170–181.
- Melluso, L., Mahoney, J.J., Dallai, L., 2006. Mantle sources and crustal input as recorded in high-mg Deccan traps basalts of Gujarat (India). *Lithos* 89 (3–4), 259–274.

- Metcalfe, I., 2002. Permian tectonic framework and palaeogeography of SE Asia. *Journal of Asian Earth Sciences* 20 (6), 551–566.
- Metcalfe, I., 2006. Paleozoic and Mesozoic tectonic evolution and palaeogeography of east Asian crustal fragments: the Korean peninsula in context. *Gondwana Research* 9 (1–2), 24–46.
- Metcalfe, I., 2013. Gondwana dispersion and Asian accretion: tectonic and palaeogeographic evolution of eastern Tethys. *Journal of Asian Earth Sciences* 66 (2013), 1–33.
- Miller, C., Thoni, M., Frank, W., Grasemann, B., Klotzli, U., Guntli, P., Draganits, E., 2001. The early Palaeozoic magmatic event in the northwest Himalaya, India: source, tectonic setting and age of emplacement. *Geology Magazine* 138, 237–251.
- Mitchell, A.L., Grove, T.L., 2015. Melting the hydrous, subarc mantle: the origin of primitive andesites. *Contributions to Mineralogy and Petrology* 170 (2).
- Nam, T.N., Toriumi, M., Sano, Y., Terada, K., Thang, T.T., 2003. 2.9, 2.36, and 1.96 Ga zircons in orthogneiss south of the Red River shear zone in Viet Nam: evidence from SHRIMP U-Pb dating and tectonothermal implications. *Journal of Asian Earth Sciences* 21 (7), 743–753.
- Nie, X.M., Feng, Q.L., Qian, X., Wang, Y.J., 2015. Magmatic record of Prototethyan evolution in SW Yunnan, China: geochemical, zircon U-Pb geochronological and Lu-Hf isotopic evidence from the Huimin metavolcanic rocks in the southern Lancangjiang zone. *Gondwana Research* 28 (2), 757–768.
- Niu, Y.L., Wilson, M., Humphreys, E.R., O'Hara, M.J., 2012. A trace element perspective on the source of ocean island basalts (OIB) and fate of subducted ocean crust (SOC) and mantle lithosphere (SML). *Episodes* 35 (2), 310–327.
- Pecerillo, A., Barberio, M.R., Yirgu, G., Ayalew, D., Barbieri, M., Wu, T.W., 2003. Relationships between mafic and peralkaline silicic magmatism in continental rift settings: a petrological, geochemical and isotopic study of the Gedemsa volcano, central Ethiopian rift. *Journal of Petrology* 44 (11), 2003–2032.
- Peng, T.P., Wilde, S.A., Fan, W.M., Peng, B.X., 2013. Neoarchean siliceous high-mg basalt (SHMB) from the Taishan granite-greenstone terrane, eastern North China Craton: Petrogenesis and tectonic implications. *Precambrian Research* 228, 233–249.
- Petrone, C.M., Ferrari, L., 2008. Quaternary adakite - Nb-enriched basalt association in the western trans-Mexican Volcanic Belt: is there any slab melt evidence? *Contributions to Mineralogy and Petrology* 156 (1), 73–86.
- Qi, X.X., Zeng, L.S., Zhu, L.H., Hu, Z.C., Hou, K.J., 2012. Zircon U-Pb and Lu-Hf isotopic systematics of the Daping plutonic rocks: implications for the Neoproterozoic tectonic evolution of the northeastern margin of the Indochina block, Southwest China. *Gondwana Research* 21 (1), 180–193.
- Qi, X.X., Santosh, M., Zhu, L.H., Zhao, Y.H., Hu, Z.C., Zhang, C., Ji, F.B., 2014. Mid-Neoproterozoic arc magmatism in the northeastern margin of the Indochina block, SW China: Geochronological and petrogenetic constraints and implications for Gondwana assembly. *Precambrian Research* 245, 207–224.
- Rapp, R.P., Watson, E.B., 1995. Dehydration melting of Metabasalt at 8–32-kbar—implications for continental growth and crust-mantle recycling. *Journal of Petrology* 36 (4), 891–931.
- Redman, B.A., Keays, R.R., 1985. Archaean basic volcanism in the eastern Goldfields Province, Yilgarn block, Western Australia. *Precambrian Research* 30, 113–152.
- Shi, M.F., Lin, F.C., Fan, W.Y., Deng, Q., Cong, F., Tran, M.D., Zhu, H.P., Wang, H., 2015. Zircon U-Pb ages and geochemistry of granitoids in the Truong son terrane, Vietnam: tectonic and metallogenetic implications. *Journal of Asian Earth Sciences* 101, 101–120.
- Straub, S.M., Gomez-Tuena, A., Zellmer, G.F., Espinasa-Pereira, R., Stuart, F.M., Cai, Y., Langmuir, C.H., Martin-Del Pozzo, A., Mesko, G.T., 2013. The processes of melt differentiation in arc volcanic rocks: insights from OIB-type arc magmas in the central Mexican Volcanic Belt. *Journal of Petrology* 54 (4), 665–701.
- Sun, S.S., McDonough, W.F., 1989. Chemical and isotopic systematics of oceanic basalts: implication for mantle composition and process. *Geological Society, London, Special Publications* 42 (SI), 313–345.
- Thanh, T.D., Janvier, P., Phuong, T.H., 1996. Fish suggests continental connections between the Indochina and South China blocks in middle Devonian time. *Geology* 24 (6), 571–574.
- Thanh, N.X., Hai, T.T., Hoang, N., Lan, V.Q., Kwon, S., Itaya, T., Santosh, M., 2014. Backarc mafic-ultramafic magmatism in northeastern Vietnam and its regional tectonic significance. *Journal of Asian Earth Sciences* 90, 45–60.
- Turner, S.J., Langmuir, C.H., Katz, R.F., Dungan, M.A., Escrig, S., 2016. Parental arc magma compositions dominantly controlled by mantle-wedge thermal structure. *Nature Geoscience* 9 (10), 772–776.
- Wang, X.F., Metcalfe, I., Jian, P., He, L.Q., Wang, C.S., 2000. The Jinshajiang-Ailaoshan suture zone, China: tectonostratigraphy, age and evolution. *Journal of Asian Earth Sciences* 18 (6), 675–690.
- Wang, Y.J., Fan, W.M., Zhang, Y.H., Peng, T.P., Chen, X.Y., Xu, Y.G., 2006. Kinematics and Ar-40/Ar-39 geochronology of the Gaoligong and Chongshan shear systems, western Yunnan, China: implications for early Oligocene tectonic extrusion of SE Asia. *Tectonophysics* 418 (3–4), 235–254.
- Wang, C.Y., Zhou, M.F., Qi, L., 2007a. Permian flood basalts and mafic intrusions in the Jinping (SW China) song Da (northern Vietnam) district: mantle sources, crustal contamination and sulfide segregation. *Chemical Geology* 243 (3–4), 317–343.
- Wang, Q., Wyman, D.A., Zhao, Z.H., Xu, J.F., Bai, Z.H., Xiong, X.L., Dai, T.M., Li, C.F., Chu, Z.Y., 2007b. Petrogenesis of carboniferous adakites and Nb-enriched arc basalts in the Altaw area, northern Tianshan range (western China): implications for Phanerozoic crustal growth in the Central Asia orogenic belt. *Chemical Geology* 236 (1–2), 42–64.
- Wang, Q., Wyman, D.A., Xu, J.F., Wan, Y.S., Li, C.F., Zi, F., Jiang, Z.Q., Qiu, H.N., Chu, Z.Y., Zhao, Z.H., Dong, Y.H., 2008. Triassic Nb-enriched basalts, magnesian andesites, and adakites of the Qiangtang terrane (Central Tibet): evidence for metasomatism by slab-derived melts in the mantle wedge. *Contributions to Mineralogy and Petrology* 155 (4), 473–490.
- Wang, B.D., Wang, L.Q., Pan, G.T., Yin, F.G., Wang, D.B., Tang, Y., 2013a. U-Pb zircon dating of early Paleozoic gabbro from the Nantinghe ophiolite in the Changning-Menglian suture zone and its geological implication. *Chinese Science Bulletin* 58 (8), 920–930.
- Wang, Y.J., Fan, W.M., Zhang, G.W., Zhang, Y.H., 2013b. Phanerozoic tectonics of the South China block: key observations and controversies. *Gondwana Research* 23 (4), 1273–1305.
- Wang, Y.J., Zhang, A.M., Fan, W.M., Zhang, Y.H., Zhang, Y.Z., 2013c. Origin of paleo-subduction-modified mantle for Silurian gabbro in the Cathaysia block: Geochronological and geochemical evidence. *Lithos* 160, 37–54.
- Wang, Q.F., Deng, J., Li, C.S., Li, G.J., Yu, L., Qiao, L., 2014. The boundary between the Simao and Yangtze blocks and their locations in Gondwana and Rodinia: constraints from detrital and inherited zircons. *Gondwana Research* 26 (2), 438–448.
- Wang, Y.J., Zhou, Y.Z., Cai, Y.F., Liu, H.C., Zhang, Y.Z., Fan, W.M., 2016. Geochronological and geochemical constraints on the petrogenesis of the Ailaoshan granitic and migmatitic rocks and its implications on Neoproterozoic subduction along the SW Yangtze block. *Precambrian Research* 283, 106–124.
- Wang, Y.J., Qian, X., Cawood, A.P., Liu, H.C., Feng, Q.L., Zhao, G.C., Zhang, Y.H., He, H.Y., Zhang, P.Z., in press. Closure of the east Paleotethyan Ocean and amalgamation of the eastern Cimmerian and Southeast Asia continental fragments. *Earth-Science Reviews*, <https://doi.org/10.1016/j.earscirev.2017.09.013>.
- Xia, X.P., Ren, Z.Y., Wei, G.J., Zhang, L., Sun, M., Wang, Y.J., 2013. In situ rutile U-Pb dating by laser ablation-MC-ICPMS. *Geochemical Journal* 47 (4), 459–468.
- Xia, X.P., Nie, X.S., Lai, C.K., Wang, Y.J., Long, X.P., Meffre, S., 2016. Where was the Ailaoshan Ocean and when did it open: a perspective based on detrital zircon U-Pb age and Hf isotope evidence. *Gondwana Research* 36, 488–502.
- Xing, X.W., Wang, Y.J., Cawood, A.P., Zhang, Y.Z., 2016. Early Paleozoic accretionary orogenesis along northern margin of Gondwana constrained by high-Mg metaigneous rocks. *SW Yunnan, International Journal of Earth Sciences* 106 (5), 1–18.
- Xu, J.F., Castillo, P.R., 2004. Geochemical and Nd-Pb isotopic characteristics of the Tethyan asthenosphere: implications for the origin of the Indian Ocean mantle domain. *Tectonophysics* 393 (1–4), 9–27.
- Xu, Y.G., Chung, S.L., Jahn, B.M., Wu, G.Y., 2001. Petrologic and geochemical constraints on the petrogenesis of Permian-Triassic Emeishan flood basalts in southwestern China. *Lithos* 58 (3–4), 145–168.
- Yang, T.N., Ding, Y., Zhang, H.R., Fan, J.W., Liang, M.J., Wang, X.H., 2014. Two-phase subduction and subsequent collision defines the Paleotethyan tectonics of the southeastern Tibetan plateau: evidence from zircon U-Pb dating, geochemistry, and structural geology of the Sanjiang orogenic belt, Southwest China. *Geological Society of America Bulletin* 126, 1654–1682.
- Yunnan BGMR, 1990. *Regional Geology of Yunnan Province (in Chinese)*. Geology Publishing House, Beijing, pp. 273–428.
- Zaw, K., Meffre, S., Lai, C.K., Burrett, C., Santosh, M., Graham, I., Manaka, T., Salam, A., Kamvong, T., Cromie, P., 2014. Tectonics and metallogeny of mainland Southeast Asia - a review and contribution. *Gondwana Research* 26 (1), 5–30.
- Zhang, Z.C., Mahoney, J.J., Mao, J.W., Wang, F.H., 2006. Geochemistry of picritic and associated basalt flows of the western Emeishan flood basalt province, China. *Journal of Petrology* 47 (10), 1997–2019.
- Zhang, R.Y., Lo, C.H., Chung, S.L., Grove, M., Omori, S., Izuka, Y., Liou, J.G., Tri, T.V., 2013. Origin and tectonic implication of Ophiolite and Eclogite in the song ma suture zone between the South China and Indochina blocks. *Journal of Metamorphic Geology* 31, 49–62.
- Zhang, R.Y., Lo, C.H., Li, X.H., Chung, S.L., Anh, T.T., Tri, T.T., 2014. U-Pb dating and tectonic implication of ophiolite and metabasite from the song ma suture zone, northern Vietnam. *American Journal of Sciences* 314, 649–678.
- Zhong, D.L., 1998. *The Paleotethysides in West Yunnan and Sichuan*. Science Press, Beijing, pp. 1–230 (in Chinese).
- Zhu, D.C., Wang, Q., Zhao, Z.D., Chung, S.L., Cawood, P.A., Niu, Y.L., Liu, S.A., Wu, F.Y., Mo, X., 2015. Magmatic record of India-Asia collision. *Scientific Reports* 5, 1–8.
- Zi, J.W., Fan, W.M., Wang, Y.J., Peng, T.P., Guo, F., 2008. Geochemistry and petrogenesis of the Permian mafic dykes in the Panxi region, SW China. *Gondwana Research* 14 (3), 368–382.
- Zi, J.W., Cawood, P.A., Fan, W.M., Wang, Y.J., Tohver, E., 2012. Contrasting rift and subduction-related plagiogranites in the Jinshajiang ophiolitic melange, Southwest China, and implications for the paleo-Tethys. *Tectonics* 31 (2), 1–18.